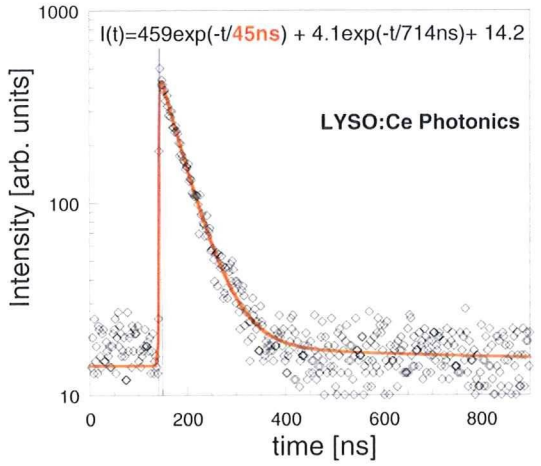

Fig. 9. Spectrally unresolved scintillation decay at RT. Solid line is the convolution of instrumental response (also in the figure) with the function I(t) given in the figure.

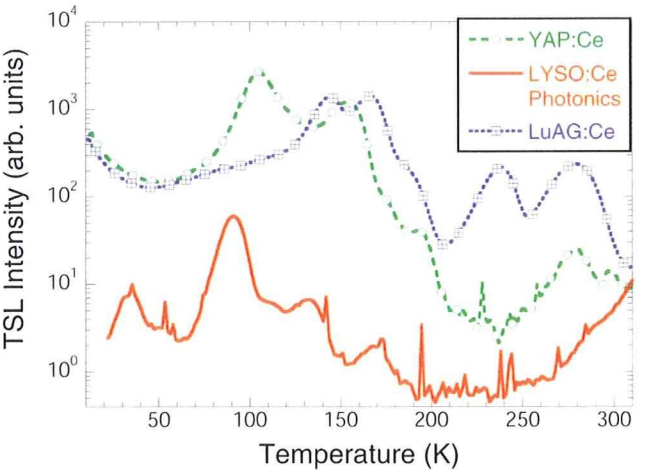

Fig. 10. TSL glow curves of YAP:Ce, LuAG:Ce and LYSO:Ce after X-irradiation at 10 K. Curves can be compared quantitatively.

C. Ce-Doped Orthosilicates

Scintillation characteristics of Ce-doped rare-earth (RE) oxyorthosilicates were for Gd_2SiO_5:Ce (GSO) reported more than 20 years ago [31]. Optical studies of Ce-doped samples showed two Ce^{3+} emission bands related to two different Ce^{3+} crystallographic sites in GSO, LSO, and YSO [32]. In LSO:Ce the doublet emission peaking at 393 nm and 427 nm was ascribed to "Ce_1" center, the luminescence of which is not quenched up to RT. On the other hand, the composite emission peaking at 460 nm, well detected only below 80 K, was ascribed to the "Ce_2" center. The presence of two distinct Ce^{3+} emissions is in accordance with the existence of two Lu^{3+} crystallographic sites and with the incorporation of Ce as a substitute for Lu. ESR measurements support this assumption since Ce^{3+} ions are found at both lutetium sites. As the ESR intensity is directly linked to the concentration of paramagnetic ions, the relative Ce^{3+} concentration in each site could have been determined. The values are: $Ce_1 = 95\%$ and $Ce_2 = 5\%$. The most substituted site is attributed to the larger Lu_1 site with $6+1$ oxygen neighbors [33].

In contrast to aluminum perovskites and garnets the scintillation decay of Ce-doped LSO or LYSO shows the only component with the decay time somewhat longer with respect to the PL one (35 ns), Fig. 9. Moreover, there is practically no difference between the decays of Ce-doped LSO and LYSO (with a typical 5–10% of Y admixing).

TSL glow curve of LYSO:Ce with a relatively high LY (Photonics Material, see ref. 34 for LY measurements) is displayed in Fig. 10 together with those of LuAG:Ce and YAP:Ce. Concentration of Ce^{3+} in these YAP, LYSO and LuAG samples is determined from the optical absorption spectra and using an ICP chemical analysis of about 8000 ppm, 1300 ppm and 2400 ppm, respectively. One can immediately see that the amplitude of TSL signal in LYSO:Ce is 1–2 orders of magnitude lower with respect to that of the other two samples indicating the lack of shallow electron traps in silicates with respect to aluminum perovskite and garnet hosts. This is consistent with the absence of slower decay components in LYSO:Ce scintillation response (Fig. 10).

Another advantage of LSO host consists in low thermal stability of intrinsic emission centres based on self-trapped excitons or holes, which persist only up to about 50 K, and then are thermally disintegrated [35]. Thus host-related slower emissions do not delay an energy transfer towards Ce^{3+} in any noticeable manner, while emission related to the presence of AD in YAG/LuAG host survives up to RT and is in competition with that of Ce^{3+} under high energy excitation [36].

In the case of LSO, it was soon recognized that it presents a fairly strong afterglow at RT [37]. Fundamental studies focusing on the comprehension of the microscopic physical mechanism governing afterglow were carried out in order to find possible technological solutions. The activation energy of the process was found to be approximately 1 eV [37]; it is in accordance with the calculated trap depth of the leading TSL peak situated at 375 K and 340 K (using a heating rate of 6 K/s and 0.24K/s, respectively). Hence, mentioned afterglow appears to be due to RT carrier detrapping from the trap responsible for this TSL peak followed by radiative recombination at Ce^{3+} luminescent centers. Actually the 340 K peak (heating rate 0.24 K/s) is the first one of a series of as many as 6 peaks observed in the glow curve above RT, Fig. 11. Its spectral emission coincides with the Ce^{3+} 5d-4f transition [37]. Annealing experiments in reducing or oxidizing atmosphere led to the suggestion that traps could be related to oxygen vacancies [38]. Indeed, TSL glow curves above RT show a very similar pattern for both LSO and LYSO samples coming from different manufacturers, Fig. 11. Evaluation of the trap depth for all of the glow peaks in LYSO:Ce (G.Ren) sample in Fig. 11 was made using the partial cleaning method, see e.g., [39], [40] for details, and the obtained values are reported in Fig. 12. Interestingly, with the exception of the 305°C peak of the trap depth of about 1.5 eV, the trap depth within 30–260°C is very little temperature dependent in contrast to usual situation, in which a step-like dependence of the trap-depth on increasing temperature is obtained (for LuAG:Ce see [40]). A very similar situation was found in YAP:Ce and LuYAP:Ce [39] and was explained as due to a thermally assisted tunnelling of electrons trapped at oxygen vacancies towards holes trapped at Ce ions at discrete distances (given by

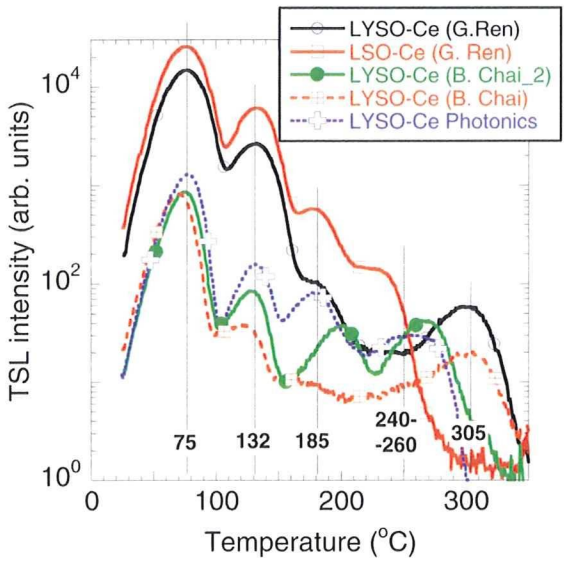

Fig. 11. TSL glow curves after X-irradiation at RT at LSO:Ce and LYSO:Ce.

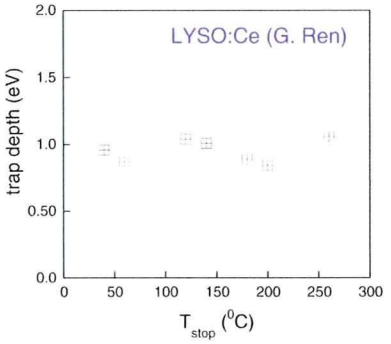

Fig. 12. Temperature dependence of the trap depth on $T_{\rm stop}$ in the partial cleaning procedure, for details see [39].

the crystal structure), followed by their radiative recombination. The same consideration can be done in LSO(LYSO):Ce so that it is tentatively proposed that such thermally assisted tunneling between an oxygen vacancy-based electron trap and $\mathrm{Ce_1}$ hole trap is responsible for the observed TSL glow curve pattern above RT up to some 260°C.

IV. Conclusions

Participation of various trapping states in the aluminum perovskites and garnets and in the orthosilicate scintillators was studied by correlated experiments using time-resolved luminescence spectroscopy and thermoluminescence.

Dominating shallow electron trap in aluminum garnets is ascribed to the $\mathrm{Y_{Al}}$ and $\mathrm{Lu_{Al}}$ antisite defects, which gives rise to the 92 K and triple 142–165-190 K TSL glow curve peaks, respectively. At RT the calculated detrapping times from related traps to conduction band for LuAG:Ce are longer than $\sim 50\ \mu$s, so that this mechanism cannot be responsible for the existence of slower submicrosecond component in LuAG:Ce scintillation decay. Due to the evidence of tunneling-driven radiative recombination in the spatially correlated $\mathrm{Ce^{3+}}$-AD pairs at low temperatures, this mechanism is proposed to explain the observed scintillation decay pattern at RT as well.

At RT the detrapping times related to the 105 K and 150 K TSL peaks in YAP:Ce are of the same order as those related to the antisite-defect related trap in LuAG:Ce and the absolute intensity of peaks is comparable as well. However, relative amplitude of the glow curve peaks within 200–300 K is noticeably higher in LuAG:Ce, which might be the reason for its lower LY.

Admixture of Lu into YAP host results in the high temperature shift and amplitude increase of the dominant 105 K peak. TSL intensity between 200–300 K is enhanced as well. All these phenomena can increase detrapping times at RT and effectively lower the light yield values. However, consistent TSL study over the full concentration range of the YAP-LuAP solid solution is necessary to understand in detail particular features of energy transfer and capture in the mixed systems.

Quantitative comparison of low temperature TSL glow curves among the Ce-doped aluminum perovskites, garnets and orthosilicates points to the lack of shallow electron traps in orthosilicates resulting in faster energy transfer from the host towards the $\mathrm{Ce^{3+}}$ ions. Another advantage of orthosilicate host is due to comparatively lower thermal stability of self-trapped exciton and hole states. These states become thermally disintegrated above 50 K and enable faster energy migration to the $\mathrm{Ce^{3+}}$ ions in comparison with aluminum garnets. These two factors are recognized as crucial in explanation of higher light yield values obtained at LSO:Ce and LYSO:Ce.

Temperature independence of trap depth corresponding to the TSL glow curve peaks within 40–260°C in LSO:Ce and LYSO:Ce cannot be explained by usual detrapping mechanism via conduction band. Instead, thermally assisted tunneling mechanism is proposed to explain the observed features similarly as earlier reported in the literature for YAP:Ce.

Obtained results point to possible space correlation and relative vicinity between the emission center ($\mathrm{Ce^{3+}}$, $\mathrm{Pr^{3+}}$) and an electron trap (antisite defect, oxygen vacancy or other) in most of the material studied. The mechanism of such impurity ion-defect aggregation is not clear and is worth further investigation.

References

[1] M. Nikl, "WIDE BAND GAP SCINTILLATION MATERIALS. Progress in the technology and material understanding," *Phys. Stat. Sol. (a)*, vol. 178, pp. 595–620, 2000.

[2] C. W. E. v. Eijk, "Inorganic-scintillator development," *Nucl. Instrum. Methods Phys. Res. A*, vol. A460, pp. 1–14, 2001.

[3] K. W. Kramer, P. Dorenbos, H. U. Gudel, and C. W. E. v. Eijk, "Development and characterization of highly efficient new cerium doped rare earth halide scintillator materials," *J. Mater. Chem.*, vol. 16, pp. 2773–2780, 2006.

[4] M. Nikl, "Scintillation detectors for x-rays," *Meas. Sci. Technol.*, vol. 17, pp. R37–R54, 2006.

[5] R. Autrata, P. Schauer, J. Kvapil, and J. Kvapil, "A single crystal of YAG—New fast scintillator in SEM," *J. Phys. E, Sci. Instrum.*, vol. 11, pp. 707–708, 1978.

[6] M. Moszynski, T. Ludziewski, D. Wolski, W. Klamra, and L. O. Norlin, "Properties of the YAG:Ce scintillator," *Nucl. Instrum. Methods Phys. Res. A*, vol. A345, pp. 461–467, 1994.

[7] A. Lempicki, M. H. Randles, D. Wisniewski, M. Balcerzyk, C. Brecher, and A. J. Wojtowitz, "$\mathrm{LuAlO_3}$:Ce and other aluminate scintillators," *IEEE Trans. Nucl. Sci.*, vol. 42, no. 4, pp. 280–284, Aug. 1995.

[8] M. Nikl, E. Mihokova, J. A. Mares, A. Vedda, M. Martini, K. Nejezchleb, and K. Blazek, "Traps and timing characteristics of $\mathrm{LuAG:Ce^{3+}}$ scintillator," *Phys. Stat. Sol. (b)*, vol. 181, pp. R10–R12, 2000.

[9] M. Nikl, H. Ogino, A. Krasnikov, A. Beitlerova, A. Yoshikawa, and T. Fukuda, "Photo- and radioluminescence of Pr-doped $\mathrm{Lu_3Al_5O_{12}}$ single crystal," *Phys. Stat. Sol. (a)*, vol. 202, pp. R4–R6, 2005.

[10] H. Ogino, A. Yoshikawa, M. NIkl, K. Kamada, and T. Fukuda, "Scintillation characteristics of Pr-doped $Lu_3Al_5O_{12}$ single crystals," *J. Cryst. Growth*, vol. 287, pp. 335–338, 2006.

[11] M. Nikl, "Energy transfer in the luminescence of wide band-gap scintillators," *Phys. Stat. Sol. (a)*, vol. 202, pp. 201–206, 2005.

[12] M. Nikl, E. Mihokova, J. Pejchal, A. Vedda, Y. Zorenko, and K. Nejezchleb, "The antisite lual defect-related trap in $Lu_3Al_5O_{12}$:Ce single crystal," *Phys. Stat. Sol. (b)*, vol. 242, pp. R119–R121, 2005.

[13] M. Nikl, J. Pejchal, E. Mihokova, J. A. Mares, H. Ogino, A. Yoshikawa, T. Fukuda, and A. V. D'Ambrosio, "Antisite defect-free $Lu_3(Ga_xAl_{1-x})_5O_{12}$:Pr scintillator," *Appl. Phys. Lett.*, vol. 88, pp. 141916–141916, 2006.

[14] M. K. Ashurov, Y. K. Voronko, V. V. Osiko, A. A. Sobol, and M. I. Timoshechkin, "Spectroscopic study of stoichiometric deviationin crystals with garnet structure," *Phys. Stat. Sol. (a)*, vol. 42, pp. 101–110, 1977.

[15] C. R. Stanek, K. J. McClellan, M. R. Levy, and R. W. Grimes, "Extrinsic defect structure of $Re_3AQl_5O_{12}$ garnets," *Phys. Stat. Sol. (b)*, vol. 243, pp. R75–R77, 2006.

[16] M. Nikl, V. V. Laguta, and A. Vedda, "Energy transfer and charge carrier capture processes in wide-band-gap scintillators," *Phys. Stat. Sol. (a)*, vol. 204, pp. 683–689, 2007.

[17] H. Ogino, K. Kamada, A. Yoshikawa, J. Pejchal, J. A. Mares, M. Nikl, A. Vedda, J. Shimoyama, and K. Kishio, "Suppression of host luminescence in the Pr:LuAG scintillator," *IEEE Trans. Nucl. Sci.*, vol. 55, no. 3, Jun. 2008.

[18] Y. N. Xu and W. Y. Ching, "Electronic structure of yttrium aluminium garnet," *Phys. Rev. B*, vol. 59, pp. 10530–10535, 1999.

[19] M. J. Weber, "Optical spectra of Ce^{3+} and Ce^{3+}-sensitized fluorescence in $YAlO_3$," *J. Appl. Phys.*, vol. 44, pp. 3205–3208, 1973.

[20] T. Takeda, T. Miyata, F. Muramatsu, and T. Tomiki, "Fast decay U.V. phosphor-$YAlO_3$:Ce," *J. Electrochem. Soc.*, vol. 127, pp. 438–444, 1980.

[21] E. Autrata, P. Schauer, J. Kvapil, and J. Kvapil, "A single crystal of $YAlO_3$:Ce^{3+} as a fast scintillator in SEM," *Scanning*, vol. 5, pp. 91–96, 1983.

[22] V. G. Baryshevski *et al., Nucl. Tracks Rad. Meas.*, vol. 22, pp. 11–14, 1993.

[23] J. A. Mareš, M. Nikl, J. Chval, I. Dafinei, P. Lecoq, and J. Kvapil, "Fluorescence and scintillation properties of $LuAlO_3$:Ce crystal," *Chem. Phys. Lett.*, vol. 241, pp. 311–316, 1995.

[24] A. Mares, N. Cechova, M. Nikl, J. Kvapil, R. Kratky, and J. Pospisil, "J. Pospisil: Cerium-doped $RE^{3+}AlO_3$ perovskite scintillators: Spectroscopy and radiation induced defects," *J. Alloy. Comp.*, vol. 275–277, pp. 200–204, 1998.

[25] A. G. Petrosyan, G. O. Shyrinyan, K. L. Ovanesyan, C. Pedrini, and C. Dujardin, "Bridgman single crystal growth of Ce-doped $(Lu_{1-x}Y_x)AlO_3$," *J. Cryst. Growth*, vol. 198–199, pp. 492–496, 1999.

[26] V. G. Barishevski *et al.*, "$YAlO_3$:Ce-fast-acting scintillators for detection of ionizing radiation," *Nucl. Instrum. Methods Phys. Res. B*, vol. B58, pp. 291–293, 1991.

[27] S. I. Ziegler, J. G. Rogers, V. Selivanov, and I. Sinitzin, "Characteristics of the new $YAlO_3$:Ce compared with BGO and GSO," *IEEE Trans. Nucl. Sci.*, vol. 40, no. 2, pp. 194–197, Apr. 1993.

[28] J. Trummer, E. Auffray, P. Lecoq, A. G. Petrosyan, and P. Sempere-Roldan, "Comparison of LuAP and LuYAP crystal properties from statistically significant batches produced with two different growth methods," *Nucl. Instrum. Methods Phys. Res. A*, vol. A551, pp. 339–351, 2005.

[29] M. Fasoli, I. Fontana, F. Moretti, E. Mihokova, M. Nikl, A. Vedda, Y. Zorenko, and V. Gorbenko, "Shallow traps in $YAlO_3$: Ce single crystal perovskites," *IEEE Trans. Nucl Sci.*, vol. 55, no. 3, Jun. 2008.

[30] E. Mihóková, M. Nikl, J. A. Mareš, A. Beitlerová, A. Vedda, K. Nejezchleb, K. Blažek, and C. D'Ambrosio, "Luminescence and scintillation properties of YAG:Ce single crystal and optical ceramics," *J. Lumin.*, vol. 126, pp. 77–80, 2007.

[31] K. Takagi and T. Fukazawa, "Cerium-activated Gd_2SiO_5 single crystal scintillator," *Appl. Phys. Lett.*, vol. 42, pp. 43–45, 1983.

[32] H. Suzuki, T. A. Tombrello, C. L. Melcher, and J. S. Schweizer, "UV and gamma-ray excited luminescence of cerium-doped rare-earth oxyorthosilicates," *Nucl. Instrum. Methods Phys. Res. A*, vol. A320, pp. 263–272, 1992.

[33] L. Pidol, O. Guillot-Noël, A. Kahn-Harari, B. Viana, D. Pelenc, and D. Gourier, "EPR study of Ce^{3+} ions in lutetium silicate scintillators $Lu_2Si_2O_7$ and Lu_2SiO_5," *J. Phys. Chem. Solids*, vol. 67, pp. 643–650, 2006.

[34] J. A. Mares, M. Nikl, E. Mihokova, A. Beitlerova, A. Vedda, and C. D'Ambrosio, "Scintillation response and comparison of behavior of Ce-doped garnets, perovskites and silicates," *IEEE Trans. Nucl. Sci.*, vol. 55, no. 3, Jun. 2008.

[35] D. W. Cooke, B. L. Bennett, R. E. Muenchausen, J.-K. Lee, and M. A. Nastasi, "Intrinsic ultraviolet luminescence from Lu_2O_3, Lu_2SiO_5 and Lu_2SiO_5:Ce^{3+}," *J. Lumin.*, vol. 106, pp. 125–132, 2004.

[36] M. Nikl, J. A. Mares, N. Solovieva, J. Hybler, A. Voloshinovskii, K. Nejezchleb, and K. Blazek, "Energy transfer to the Ce^{3+} centers in $Lu_3Al_5O_{12}$:Ce scintillator," *Phys. Stat. Sol. (a)*, vol. 201, pp. R41–R44, 2004.

[37] P. Dorenbos, C. W. W. van Eijk, A. J. J. Bos, and C. L. Melcher, "Afterglow and thermoluminescence properties of Lu_2SiO_5:Ce scintillation crystals," *J. Phys .Cond. Matter*, vol. 6, pp. 4167–4180, 1994.

[38] R. Visser, C. L. Melcher, J. S. Schweizer, H. Suzuki, and T. A. Tombrello, "Photostimulated luminescence and thermoluminescence of LSO scintillators," *IEEE Trans. Nucl. Sci.*, vol. 41, no. 4, pp. 689–693, Aug. 1994.

[39] A. Vedda, M. Martini, F. Meinardi, J. A. Mares, E. Mihokova, J. Chval, M. Dusek, and M. Nikl, "Tunnelling process in thermally stimulated luminescence of mixed $Lu_xY_{1-x}AlO_3$:Ce crystals," *Phys. Rev. B*, vol. 61, pp. 8081–8086, 2000.

[40] A. Vedda, D. D. Martino, M. Martini, V. V. Laguta, M. Nikl, E. Mihokova, J. Rosa, K. Nejezchleb, and K. Blazek, "Thermoluminescence of Zr-codoped $Lu_3Al_5O_{12}$:Ce crystals," *Phys. Stat. Sol. (a)*, vol. 195, pp. R1–R3, 2003.

Vacuum ultraviolet optical properties of a micro-pulling-down-method grown $Nd^{3+}:(La_{0.9},Ba_{0.1})F_{2.9}$

Marilou Cadatal,[1,2,3,*] Yusuke Furukawa,[3] Young-Seok Seo,[3] Shingo Ono,[4] Elmer Estacio,[3] Hidetoshi Murakami,[3] Yasushi Fujimoto,[3] Nobuhiko Sarukura,[3] Masahiro Nakatsuka,[3] Kentaro Fukuda,[5,6] Rayko Simura,[6] Toshihisa Suyama,[5] Akira Yoshikawa,[6] and Fumio Saito[6]

[1]*Institute for Molecular Science (IMS), Myodaiji, Okazaki, Aichi 444-8585, Japan*
[2]*The Graduate University for Advanced Studies, Hayama, Kanagawa 240-0193, Japan*
[3]*Institute of Laser Engineering Osaka University, 2-6 Yamadaoka, Suita, Osaka 565-0871, Japan*
[4]*Nagoya Institute of Technology, Gokiso, Showa, Nagoya, Aichi 466-8555, Japan*
[5]*Tokuyama Corporation, Shibuya-ku, Tokyo 150-8383, Japan*
[6]*Institute of Multidisciplinary Research for Advanced Materials Tohoku University, 2-1-1 Katahira, Aoboa-ku Sendai, 980-8577, Japan*
**Corresponding author: cadatal-m@ile.osaka-u.ac.jp*

Received December 3, 2007; accepted January 31, 2008;
posted February 28, 2008 (Doc. ID 90369); published April 7, 2008

$Nd^{3+}:(La_{1-x},Ba_x)F_{3-x}$ ($x=0.1$) is efficiently grown by the micro-pulling-down method. Characterization of its optical properties reveals that it is transparent in the vacuum ultraviolet region with an absorption edge at around 180 nm. It has fluorescence centered at 175 nm with a bandwidth of 12 nm and a lifetime of 6.1 ns as measured by a vacuum ultraviolet streak camera and spectrometer combination. It is proposed to be suitable as a vacuum ultraviolet scintillator and a potential laser material. © 2008 Optical Society of America

OCIS codes: 300.2530, 260.7210, 160.5690.

1. INTRODUCTION

Research efforts have continuously been geared toward the generation of vacuum ultraviolet (VUV) radiation from laser materials for scientific and industrial applications such as photolithography [1,2] and spectroscopy [3,4] and from scintillators for gamma ray detection [5]. While there are available VUV laser sources such as excimer lasers based on rare gas dimers like Kr_2 and Xe_2 [6,7] and frequency conversion in nonlinear crystals [8], these have limited tunability and low conversion efficiency, respectively. In 1976 Yang and DeLuca proposed the generation of VUV radiation from dipole allowed interconfigurational $d-f$ transitions in rare-earth-doped wide-bandgap fluorides [9]. This is an attractive scheme because of its simplicity, reliability, and efficiency. It is also possible to obtain good-quality laser beams, controlled adjustment of the spectral width, and multiwavelength operation from only one laser oscillator [10]. Since the first experimental verification of their proposal [11], several studies have reported luminescence from several trivalent rare-earth-doped fluorides [12–14]. Among these, Ce^{3+}-activated fluorides, particularly $Ce^{3+}:LiCaAlF_6$ [15–17] and $Ce^{3+}:LiSrAlF_6$ [18,19] have been proved to be efficient ultraviolet (UV) active media. In spite of the encouraging results delivered by these materials, transition energies are not large enough for VUV emission. Only $Nd^{3+}:LaF_3$ has been reported to lase in the VUV region [20,21]. Work on this material, however, did not progress owing to rapid saturation of the laser output brought about by loss mechanisms such as color center formation resulting from excited state absorption. Moreover, it had limited tunability and required electron beam pumping. Because of this, there is a continuing search for appropriate activator–matrix complexes and active medium–pump source combinations suitable for generating efficient VUV tunable lasers.

On the other hand, even though the number of known scintillators amounts to several hundred, new and better materials are still needed to satisfy many requirements dependent on particular applications. For example, large-sized ZnO crystal grown by the hydrothermal method has recently been shown to be a fast scintillator for extreme UV photolithography [22]. High-performance scintillators should both be fast and efficient [23]. Nd^{3+}-doped fluorides are scintillator candidates because of their characteristic decay times of the order of 10 ns arising from the parity-allowed $d-f$ transition [24]. Crystals having high light yields can also be engineered by choosing the right activator–host material combination. Their ability to emit in the VUV region is also advantageous for specific applications. For instance, gamma ray scintillators that emit VUV fluorescence are strongly required for a gas scintillation microwire stripped detector for high-resolution positron emission tomography application [25]. Material research for VUV scintillators is also ongoing.

Innovation in crystal growth methods plays an important role in developing VUV laser materials and scintillators. Classical methods for mass production of single crystals for industrial applications, for example Czochralski and Bridgman, have already been well established [26]. However, these techniques are time and raw-material consuming, especially for single-crystal material screening. It is also difficult to combine screening with the establishment of appropriate growth conditions required for

0740-3224/08/070B27-5/$15.00

high-quality crystal production [26]. The micro-pulling-down (μ-PD) method is a relatively new crystal growth technique developed mainly at Tohoku University, Japan, to meet the challenges in materials research. Recent improvements of this method made the quality of μ-PD grown crystals comparable with those prepared by Czochralski, Bridgman–Stockbarger, or other classical growth techniques [27]. Owing to a fast growth speed, a high quality crystal can be grown by using less than 1 g of raw material in 5–12 h, thereby allowing the growth of large crystals in a shorter time and at a lower cost compared with the other melt growth methods mentioned above [27]. Moreover, this method has the capability of controlling the shape of the grown crystal to produce fibers, rods, and tubes [27]. This method was initially designed for the growth of oxide crystals, and several studies have demonstrated the advantages of this method [28–30]. However, because fluoride materials have received considerable attention, innovation of the μ-PD apparatus to accommodate fluoride crystal growth was carried out. Moreover, extensive research is devoted to the improvement of this method to facilitate the screening of fluoride host lattices, dopant concentration, and optimization of the growth parameters. The demonstration of radio luminescence from μ-PD-grown Ce:PrF_3 shows that this method is capable of efficiently growing fluoride crystals [31]. In this paper, we report the successful growth of Nd^{3+}:$(La_{0.9},Ba_{0.1})F_{2.9}$ crystal by using the μ-PD method modified for fluoride crystal growth. For comparison, we have also grown Nd^{3+}:LaF_3, using the same growth parameters. The optical characteristics of these materials in the VUV region are investigated and compared. Our results not only reinforce μ-PD's merits as a useful tool for fluoride crystal growth but also advance the development of a VUV scintillator and laser material.

2. EXPERIMENTAL SETUP

Nd^{3+}:$La_{(1-x)}Ba_xF_{3-x}$ ($x=0.1$) or Nd^{3+}:$(La_{0.9},Ba_{0.1})F_{2.9}$ is grown by using the μ-PD apparatus for fluoride crystal growth shown in Fig. 1. High-purity LaF_3, BaF_2, and NdF_3 are prepared as starting materials at a molar ratio of 90:10:1. They are thoroughly mixed and placed inside a graphite crucible. The growth chamber is then evacuated to 10^{-4} Torr by rotary and diffusion pumps. Using radio frequency heating, the crucible is baked at 600°C for 1 h to remove oxygen traces from the moisture of raw materials and adsorbates on the chamber surface. Simultaneously, the chamber is further evacuated to 10^{-5} Torr. After baking, the recipient is filled with a mixture of argon and CF_4, which will serve as the growth atmosphere, until ambient pressure is reached. The crucible is then heated to the melting temperature of about 1450°C. The single crystal is grown with a pulling rate of 0.1 mm/min and with complete solidification of the melt charged in the crucible. A detailed description of the μ-PD apparatus can be found in [32]. The phase diagram for the LaF_3–BaF_2 system shows that $La_{(1-x)}Ba_xF_{3-x}$ with $0.2<x<0.5$ would be eutectic and opaque [33]. In our experiment, we observed that the crystal is already cloudy when $x=0.15$; thus we chose $x=0.1$. For reference, Nd^{3+}:LaF_3 crystal is also grown from the stoichiometric mixture of high-purity LaF_3 and NdF_3 by using the same growth parameters. For 1 mol.% Nd doping concentration, the number density of Nd^{3+} ions in $(La_{0.9},Ba_{0.1})F_{2.9}$ and LaF_3 host is 1.65×10^{20} cm^{-3} and 1.81×10^{20} cm^{-3}, respectively. The as-grown crystals are 20-mm in length and 2-mm in diameter. Both crystals have no visible cracks or inclusions. A photograph of the actual samples used in fluorescence measurements is shown in Fig. 2.

The absorption coefficient is measured by using a N_2-purged VUV spectrometer (Bunkoh-keiki, type KV-201) and a semi-double-beam system that uses a deuterium lamp. The samples used are 1 mm thick. For fluorescence measurements, an F_2 laser (MPB Tech., PSX-100) operating at 157 nm, 100 Hz repetition rate, 1 mJ pulse energy, and 5 ns pulse duration excites the sample placed inside a vacuum chamber. The optical path from the laser to the vacuum chamber is also purged with N_2 gas to prevent absorption of the 157 nm excitation by oxygen. A MgF_2 lens is used to collect and focus the fluorescence onto the entrance slit of a spectrograph. The spectrograph has a 1 nm resolution. A VUV CCD array detects the fluorescence spectrum. In all measurements, the spectrum is corrected for the CCD detector spectral response.

Temporal measurements to determine the fluorescence lifetimes of Nd^{3+}:$(La_{0.9},Ba_{0.1})F_{2.9}$ and Nd^{3+}:LaF_3 are per-

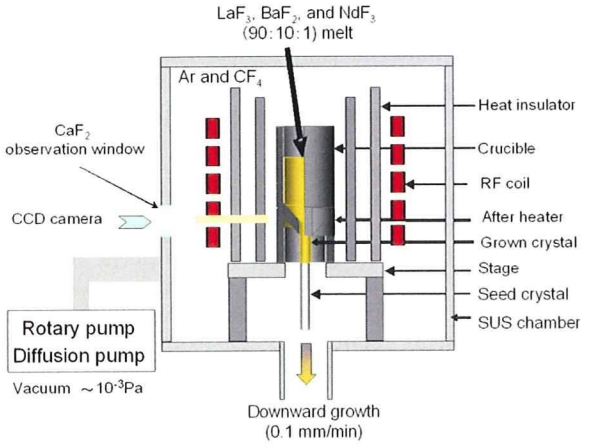

Fig. 1. (Color online) The μ-PD apparatus modified for fluoride crystal growth, used to grow Nd^{3+}:$(La_{0.9},Ba_{0.1})F_{2.9}$.

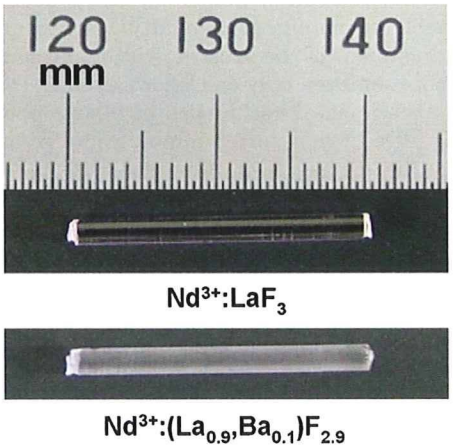

Fig. 2. (Color online) As-grown Nd^{3+}:$(La_{0.9},Ba_{0.1})F_{2.9}$ and Nd^{3+}:LaF_3 crystals.

formed with a streak camera and a Seya-Namioka VUV spectrometer combination. The spectrometer is connected to the vacuum chamber where the fluoride sample is placed. The schematic diagram of the system is shown in Fig. 3. The entire system is maintained at a vacuum level of 10^{-6} Torr. Moreover, all measurements are spectrally and temporally calibrated.

3. RESULTS

Transmission characteristics are highly influenced by the host material. Fluorides are promising because they are capable of emitting in the VUV region because of their broad bandgaps. They are also highly transparent in the VUV region. This makes them suitable not only as laser materials but also as VUV optical materials. It is also possible to achieve high doping efficiency, therefore providing more flexibility in engineering their optical properties such as light output and lifetime [34,35]. Moreover, there are nontoxic and robust hosts that can be chosen from a wide range of complex fluorides. Figure 4 shows the absorption coefficient, α, of 1 mm thick $(La_{0.9},Ba_{0.1})F_{2.9}$, LaF_3, and BaF_2 hosts in the VUV region. Their absorption edges are estimated to be about 180, about 210, and about 138 nm for $(La_{0.9},Ba_{0.1})F_{2.9}$, LaF_3, and BaF_2, respectively. Clearly, $(La_{0.9},Ba_{0.1})F_{2.9}$ has a shorter transmission edge and is more transparent in the VUV region compared with LaF_3. This indicates that it will have better VUV transmission characteristics, given the same doping ion. Moreover, its short-wavelength transmission edge makes it more suitable as a short-wavelength solid-state optical material.

Figure 5 shows the VUV fluorescence from μ-PD-method-grown Nd^{3+}:$(La_{0.9},Ba_{0.1})F_{2.9}$. The plot also shows the 157 nm excitation for reference. This is the excitation that is detected after being scattered from the surface of the sample. After considering the energy levels for Nd^{3+} activator ions, the dominant peak located at 175 nm may be attributed to the allowed dipole transition from the $4f^25d$ configuration to the $^4I_{15/2}$ multiplet of the

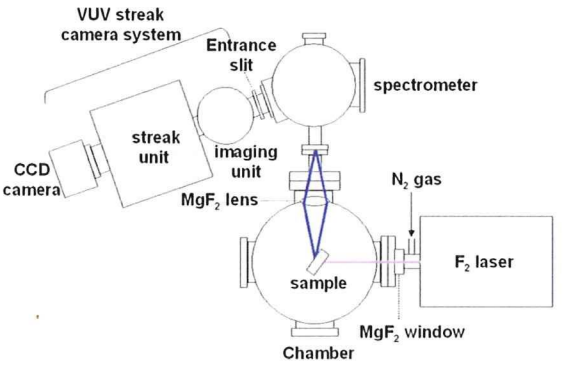

Fig. 3. (Color online) Schematic diagram of the VUV spectrometer and streak camera system used to measure the temporal characteristics of micro-PD-method-grown Nd^{3+}:$(La_{0.9},Ba_{0.1})F_{2.9}$ and Nd^{3+}:LaF_3. Measurements are carried out under a vacuum level of 10^{-6} Torr.

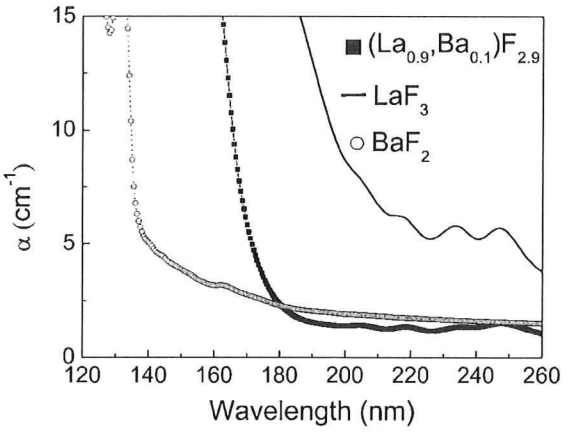

Fig. 4. Absorption coefficient, α, of undoped $(La_{0.9},Ba_{0.1})F_{2.9}$, LaF_3, and BaF_2. $(La_{0.9},Ba_{0.1})F_{2.9}$ is more transparent in the VUV region. It has an absorption edge at 180 nm compared, with LaF_3 with an absorption edge at 210 nm.

$4f^8$ configuration [36]. Using the same setup, the fluorescence spectrum from Nd^{3+}:LaF_3 is obtained. This is also shown in the same figure. The VUV fluorescence peak is located at around 172 nm, which is in good agreement with previous reports [20,21]. Both samples have the same dimensions and are grown by the same technique. The shift of the Nd^{3+}:$(La_{0.9},Ba_{0.1})F_{2.9}$ fluorescence peak to a longer wavelength compared with Nd^{3+}:LaF_3 may be due to the effect of BaF_2. The transmission of a BaF_2 host is shown in Fig. 4 for reference. Nd^{3+}:$(La_{0.9},Ba_{0.1})F_{2.9}$ is observed to have a broader fluorescence compared with Nd^{3+}:LaF_3. It has a fluorescence bandwidth (full width at half-maximum) of 12 nm, while Nd^{3+}:LaF_3 has a bandwidth of 8 nm. In this regard, Nd^{3+}:$(La_{0.9},Ba_{0.1})F_{2.9}$ will have better laser characteristics in terms of better tunability and the capability for amplification of shorter pulses. For instance, with a bandwidth of 12 nm, about 4.25 fs pulses can be amplified, while an 8 nm bandwidth could amplify about 3.7 fs pulses. Moreover, laser emission from Nd^{3+}:$(La_{0.9},Ba_{0.1})F_{2.9}$ has better prospects, since this material is transparent at the175 nm emission. A detailed discussion of the advantages of this material over Nd^{3+}:LaF_3 can be found in [32].

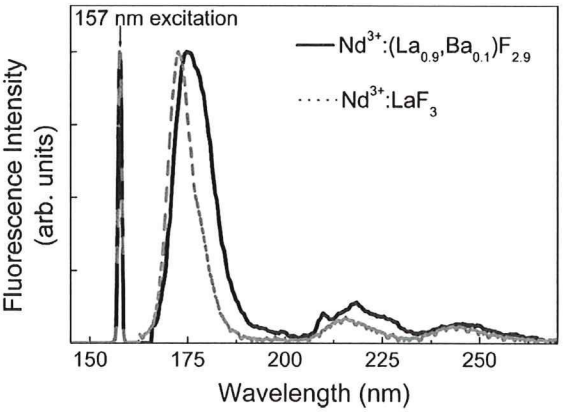

Fig. 5. F_2-laser-induced fluorescence from Nd^{3+}:$(La_{0.9},Ba_{0.1})F_{2.9}$ (solid curve) and Nd^{3+}:LaF_3 (dashed curve) with peaks at 175 and 172 nm, respectively. The spectra are corrected for the spectrograph and CCD detector spectral responses.

The streak camera image of the (157 nm emission) F_2-laser-induced Nd^{3+}:LaF_3 fluorescence is shown in Fig. 6. Also shown in the same figure is the 157 nm excitation pulse for reference. The location of the fluorescence peak is in good agreement with the spectrum that was measured by a VUV spectrograph and CCD array detector as shown in Fig. 5. The temporal profiles of the VUV fluorescence from Nd^{3+}:$(La_{0.9},Ba_{0.1})F_{2.9}$ and Nd^{3+}:LaF_3 are shown in Fig. 7. The fluorescence peak at 175 nm from Nd^{3+}:$(La_{0.9},Ba_{0.1})F_{2.9}$ has a lifetime of 6.1 ns. On the other hand, the 172 nm fluorescence from Nd^{3+}:LaF_3 has a lifetime of 8.9 ns. Fluorescence decay from both samples are single exponential. The leveling off beyond 30 ns observed from Nd^{3+}:$(La_{0.9},Ba_{0.1})F_{2.9}$ is due to background noise. Also shown in the same figure is the temporal profile of the 157 nm F_2 laser excitation pulse. It has a pulsewidth of 5 ns. The time scale of the excitation pulse is shifted to coincide with the fluorescence for clarity. In terms of scintillation properties, Figs. 4 and 7 show that Nd^{3+}:$(La_{0.9},Ba_{0.1})F_{2.9}$ is more suitable as a VUV scintillator. It is transparent at the emission wavelength, thereby resulting in better light yield. It also has a faster fluorescence decay time.

4. SUMMARY

In summary, we have successfully grown a Nd^{3+}:$(La_{0.9},Ba_{0.1})F_{2.9}$ crystal by using the μ-PD method. Investigation of its VUV optical properties in terms of transmittance, F_2-laser-induced fluorescence, and lifetime reveal that it offers several advantages over Nd^{3+}:LaF_3. For instance, it is more transparent in the VUV region with a short-wavelength absorption edge at around 180 nm. Moreover, it has a fluorescence peak at 175 nm with a bandwidth of 12 nm. These make it a potential laser material with better tunability and with the capability for amplification of shorter pulses. Moreover, it has good prospects as a VUV scintillator because of a fast fluorescence decay time and transparency in the VUV region.

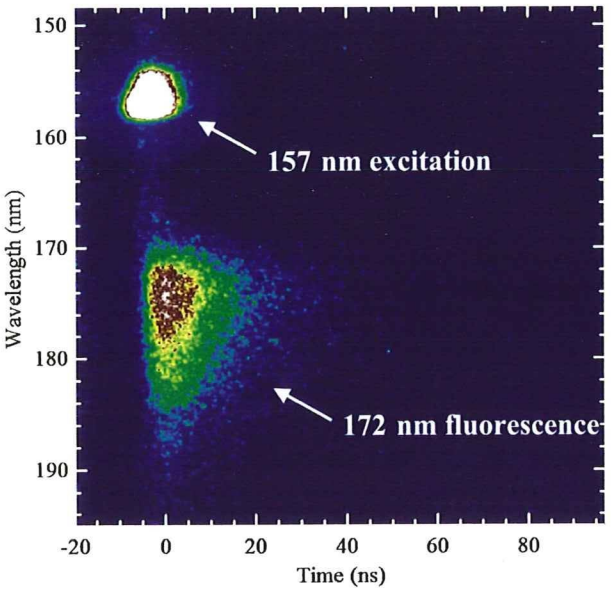

Fig. 6. (Color online) VUV streak camera image of the 172 nm fluorescence from a Nd^{3+}:LaF_3 crystal excited by a F_2 laser. Also shown is the streak camera image of the 157 nm excitation pulse. The image is temporally and spectrally calibrated.

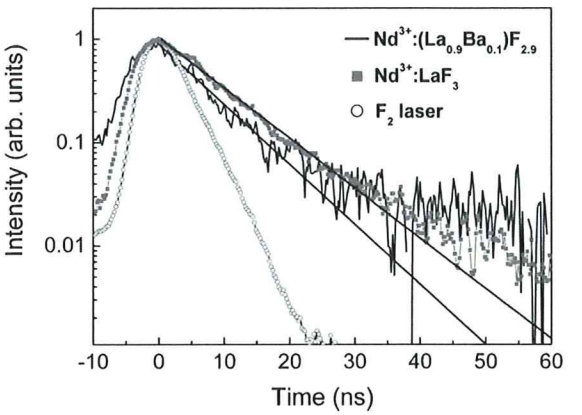

Fig. 7. The 172 nm fluorescence from Nd^{3+}:LaF_3 has a lifetime, τ, of 8.9 ns, while the 175 nm fluorescence from Nd^{3+}:$(La_{0.9},Ba_{0.1})F_{2.9}$ decays faster with a lifetime of 6.1 ns. Also shown is the temporal profile of the excitation pulse with a pulsewidth of 5 ns. The excitation pulse is shifted to have the same time scale as the fluorescence for clarity.

ACKNOWLEDGMENTS

This work was partially supported by the Ministry of Education, Culture, Sports, Science, and Technology of Japan, Grant-in-Aid for Young Scientists (A), 19686001, 2007. We thank Tsuguo Fukuda from the Institute of Multidisciplinary Research for Advanced Materials (IMRAM), Tohoku University, for his useful discussions and suggestions.

REFERENCES

1. T. Suganuma, H. Kubo, O. Wakabayashi, H. Mizoguchi, K. Nakao, Y. Nabekawa, T. Togashi, and S. Watanabe, "157-nm coherent light source as an inspection tool for F_2 laser lithography," Opt. Lett. **27**, 46–48 (2002).
2. R. H. French, R. C. Wheland, D. J. Jones, J. N. Hilfiker, R. A. Synowicki, F. C. Zumsteg, J. Feldman, and A. E. Feiring, "Fluoropolymers for 157 nm lithography: optical properties from VUV absorbance and ellipsometry measurements," Proc. SPIE **4000**, 1491–1502 (2000).
3. L. Skuja, K. Kajihara, M. Hirano, and H. Hosono, "Fluorine laser-induced silicon hydride Si–H groups in silica," J. Non-Cryst. Solids **353**, 526–529 (2007).
4. R. H. French, D. J. Jones, H. Müllejans, S. Loughin, A. D. Dorneich, and P. F. Carcia, "Optical properties of aluminum nitride: determined from vacuum ultraviolet spectroscopy and spectroscopic ellipsometry," J. Mater. Res. **14**, 4337–4344 (1999).
5. V. N. Makhov, N. Yu. Kirikova, M. Kirm, J. C. Krupa, P. Liblik, A. Lushchik, Ch. Lushchik, E. Negodin, and G. Zimmerer, "Luminescence properties of YPO_4:Nd^{3+}: a promising VUV scintillator material," Nucl. Instrum. Methods Phys. Res. A **486**, 437–442 (2002).
6. W. Sasaki, T. Shirai, S. Kubodera, J. Kawanaka, and T. Igarashi, "Observation of vacuum-ultraviolet $Kr_{2}*$ laser oscillation pumped by a compact discharge device," Opt. Lett. **26**, 503–505 (2001).
7. R. H. Lipson and P. E. LaRocque, "Vacuum ultraviolet laser-excited spectra of Xe_2," Opt. Lett. **9**, 402–404 (1984).
8. C. T. Chen, J. Lu, T. Togashi, T. Suganuma, T. Sekikawa, S.

Watanabe, Z. Xu, and J. Wang, "Second-harmonic generation from a $KBe_2BO_3F_2$ crystal in the deep ultraviolet," Opt. Lett. **27**, 637–639 (2002).
9. K. H. Yang and J. A. DeLuca, "VUV fluorescence of Nd^{3+}-, Er^{3+}-, and Tm^{3+}-doped trifluorides and tunable coherent sources from 1650 to 2600 Å," Appl. Phys. Lett. **29**, 499–501 (1976).
10. R. Moncorge, "Spectroscopy of broad-band UV-emitting materials based on trivalent rare-earth ions," in *Ultraviolet Spectroscopy and UV Lasers*, M. A. Dubinskii and P. Misra, eds. (Marcel and Drekker, 2002), pp. 337–395.
11. D. J. Ehrlich, P. F. Moulton, and R. M. Osgood, Jr., "Ultraviolet solid-state Ce:YLF laser at 325 nm," Opt. Lett. **4**, 184–186 (1979).
12. V. N. Makhov, M. N. Khaidukov, N. Yu. Kirikova, M. Kirm, J. C. Krupa, T. V. Ouvarova, and G. Zimmerer, "VUV spectroscopy of wide band-gap crystals doped with rare earth ions," Nucl. Instrum. Methods Phys. Res. A **470**, 290–294 (2001).
13. V. N. Makhov, N. M. Khaidukov, N. Yu. Kirikova, M. Kirm, J. C. Krupa, T. V. Ouvarova, and G. Zimmerer, "VUV emission of rare-earth ions doped into fluoride crystals," J. Lumin. **87–89**, 1005–1007 (2000).
14. J. C. Krupa and M. Queffelec, "UV and VUV optical excitations in wide band gap materials doped with rare earth ions: $4f-5d$ transitions," J. Alloys Compd. **250**, 287–292 (1997).
15. M. A. Dubinskii, V. V. Semashko, A. K. Naumov, R. Y. Abdulsabirov, and S. L. Korableva, "Spectroscopy of a new active medium of a solid-state UV laser with broadband single-pass gain," Laser Phys. **3**, 216–217 (1993).
16. N. Sarukura, M. A. Dubinskii, Z. Liu, V. V. Semashko, A. K. Naumov, S. L. Koraleva, R. Yu. Abdulsabirov, K. Edamatsu, Y. Suzuki, T. Itoh, and Y. Segawa, "Ce^{3+} activated fluoride crystals as prospective media for widely tunable ultraviolet ultrafast lasers with direct 10-ns pumping," IEEE J. Sel. Top. Quantum Electron. **1**, 792–804 (1995).
17. Z. Liu, T. Kozeki, Y. Suzuki, N. Sarukura, K. Shimamura, T. Fukuda, M. Hirano, and H. Hosono, "Chirped-pulse amplification of ultraviolet femtosecond pulses by use of Ce^{3+}:$LiCaAlF_6$ as a broadband solid-state gain medium," Opt. Lett. **26**, 301–303 (2001).
18. J. F. Pinto, G. H. Rosenblatt, L. Esterowitz, and G. J. Quarles, "Tunable solid-state laser action in Ce^{3+}:$LiSrAlF_6$," Electron. Lett. **30**, 240–241 (1994).
19. C. D. Marshall, S. A. Payne, J. A. Speth, W. F. Krupke, G. J. Quarles, V. Castillo, and B. H. T. Chai, "Ultraviolet laser emission properties of Ce^{3+}-doped $LiSrAlF_6$ and $LiCaAlF_6$," J. Opt. Soc. Am. B **11**, 2054–2065 (1994).
20. R. W. Waynant and P. H. Klein, "Vacuum ultraviolet laser emission from Nd^{+3}:LaF_3," Appl. Phys. Lett. **46**, 14–16 (1985).
21. M. A. Dubinskii, A. C. Cefalas, E. Sarantopoulou, S. M. Spyrou, C. A. Nicolaides, R. Y. Abdulsabirov, S. L. Korableva, and V. V. Semashko, "Efficient LaF_3:Nd^{3+}-based vacuum-ultraviolet laser at 172 nm," J. Opt. Soc. Am. B **9**, 1148–1150 (1992).
22. M. Tanaka, M. Nishikino, H. Yamatani, K. Nagashima, T. Kimura, Y. Furukawa, H. Murakami, S. Saito, N. Sarukura, H. Nishimura, K. Mima, Y. Kagamitani, D. Ehrentraut, and T. Fukuda, "Hydrothermal method grown large-sized zinc oxide single crystal as fast scintillator for future extreme ultraviolet lithography," Appl. Phys. Lett. **91**, 231117 (2007).
23. W. Drozdowski, A. Wojtowicz, D. Wisniewski, T. Lukasiewics, and J. Kisielewski, "Scintillation properties of Pr-activated $LuAlO_3$," Opt. Mater. **28**, 102–105 (2006).
24. J. Becker, J. Y. Gesland, N. Y. Kirikova, J. C. Krupa, V. N. Makhov, M. Runne, M. Queffelec, T. V. Uvarova, and G. Zimmerer, "Fast VUV emission of rare earth ions (Nd^{3+}, Er^{3+}, Tm^{3+}) in wide bandgap crystals," J. Alloys Compd. **275–277**, 205–208 (1998).
25. H. Takahashi, University of Tokyo, Tokyo, Japan (personal communication, 2006).
26. A. Novoselov, A. Yoshikawa, and T. Fukuda, "The micro-pulling down method: fast and economic solution for materials screening," Curr. Top. Cryst. Growth Res. **7**, 87–111 (2004).
27. A. Yoshikawa, M. Nikl, G. Boulon, and T. Fukuda, "Challenge and study for developing of novel single crystalline optical materials using micro-pulling-down method," Opt. Mater. **30**, 6–10 (2007).
28. B. M. Epelbaum, K. Inaba, S. Uda, and T. Fukuda, "Micro-pulling down growth studies of lead tungstate crystals: aspects of incongruent melt vaporization," J. Cryst. Growth **178**, 426–429 (2007).
29. A. Yoshikawa, T. Akagi, M. Nikl, N. Solovieva, K. Lebbou, C. Dujardin, C. Pédrini, and T. Fukuda, "$\{Y_{3-x}, Yb_x\} \times [Ga]_2(Ga)_3O_{12}$ and $\{Lu_2Yb_1\}[Al]_2(Al)_3O_{12}$ single crystals for scintillator application grown by the modified micro-pulling-down method," Nucl. Instrum. Methods Phys. Res. A **486**, 79–82 (2002).
30. A. Yoshikawa, H. Itagaki, T. Fukuda, K. Lebbou, A. El Hassouni, A. Brenier, C. Goutaudier, O. Tillement, and G. Boulon, "Synthesis, crystal growth and second harmonic generation properties of trivalent rare-earth-doped non-linear tungsten–bronze-type structure $Ba_2Na_{1-3x}RE_xNb_5O_{15}$ (RE=Sc,Y,La,Gd,Yb and Lu)," J. Cryst. Growth **247**, 148–156 (2003).
31. A. Yoshikawa, T. Satonaga, K. Kamada, H. Sato, M. Nikl, N. Solovieva, and T. Fukuda, "Crystal growth of Ce:PrF_3 by micro-pulling-down method," J. Cryst. Growth **270**, 427–432 (2004).
32. M. Cadatal, Y. S. Seo, S. Ono, Y. Furukawa, E. Estacio, H. Murakami, Y. Fujimoto, N. Sarukura, M. Nakatsuka, T. Suyama, K. Fukuda, R. Simura, and A. Yoshikawa, "Nd^{3+}:$(La_{1-x}Ba_x)F_{3-x}$ grown by micro-pulling down method as vacuum ultraviolet scintillator and potential laser material," Jpn. J. Appl. Phys., Part 1 **46**, L985–L987 (2007).
33. B. P. Sobolev and N. L. Tkachenko, "Phase diagrams of BaF_2-(Y,Ln)F_3 systems," J. Less-Common Met. **85**, 155–170 (1982).
34. J. C. Krupa and M. Queffelec, "UV and VUV optical excitations in wide band gap materials doped with rare earth ions: $4f-5d$ transitions," J. Alloys Compd. **250**, 287–292 (1997).
35. M. F. Joubert, Y. Guyot, B. Jacquier, J. P. Chaminade, and A. Garcia, "Fluoride crystals and high lying excited states of rare earth ions," J. Fluorine Chem. **107**, 235–240 (2001).
36. G. H. Dieke and H. M. Crosswhite, "The spectra of the doubly and triply ionized rare earths," Appl. Opt. **2**, 675–686 (1963).

日本結晶成長学会誌
Vol. 35, No. 2

総合報告

新規シンチレータ結晶の開発と放射線検出器としての結実；発光メカニズムの選択から受光素子の選択，アレイ化，アセンブリおよび2次元マップの撮像まで

吉川　彰[1,2]・柳田健之[1]・横田有為[1]・荻野　拓[3]

一般に，シンチレータ結晶の開発には，発光中心の選択，母結晶の設計等を検討しつつ行うが，実際に実機搭載を具現化するには，発光波長に即した受光素子の選択，シンチレータのアレイ化，アセンブリが必要となり，その道筋を経たもののみが，2次元マップの撮像に辿りつける．本報では，シンチレータ結晶の設計指針と共に，2次元マップの撮像への道程に関して例を挙げて報告する．

はじめに

放射線検出器は，陽電子断層撮像装置（PET）やX線CTに代表される核医学や，石油や鉱物資源探査装置，地雷探査装置，空港の手荷物検査機等に代表されるセキュリティ機器，電子部品の非破壊検査装置，原子炉モニタリングポストなど，広汎な分野に応用されている．これは，放射線を紫外～可視光に変換する“シンチレータ”と，その光を電気信号に変換する“受光素子”とから成っており，非破壊検査装置の性能はこの放射線検出器部分の性能に大きく依存する．

非破壊検査はどれも重要で，広範に使われているが，中でも需要が高まっているのが核医学分野の医療画像装置と言えよう．PET装置による癌診断では癌細胞の周りに集結する性質を持つブドウ糖に微量の放射性同位体を混ぜて事前に患者に投与し，そこから発するガンマ線がシンチレータにより光に変換され，その光を光電子増倍管などの受光素子が電気信号に変換し，PC等で電気信号をデータ処理することで画像等の情報を得て癌の位置を発見している．ガンマ線は，180度正反対の方向に1対2本，放出されるが，PET装置では，円周形上に放射線検出器（シンチレータと受光素子で構成）が並んでおり，ガンマ線が当たった2箇所のシンチレータが光を放ち，その光を受光素子が電気信号に変える．後段の回路でこの電気信号を全て収集し，ソフトウエアを用いて画像を再構築することになる．

シンチレータはこの様に市民社会の安全・安心を支える応用を持ち，結晶材料分野において，半導体や圧電素子に次ぐ大きな市場規模を有する．最初に工業化されたTl: NaIは1948年にHofstadter[1]によって発見された．1973年のBGOの発見以降，X線CTやPETなどの医療画像装置の開発や欧州原子核研究所（CERN）のLarge Hadron Collider（LHC）のCompact Muon Solenoid（CMS）における高精度カロリメータ用のシンチレータの要請などとも密接に関わりながらTl: CsI[2]，BaF_2[3]，$CdWO_4$[4]，CeF_3[5]，$PbWO_4$（PWO）[6,7]，Ce: Gd_2SiO_5（GSO）[8]，Ce: Lu_2SiO_5（LSO）[9-10]などの新しいシンチレータ結晶が開発されて来た．欧米を中心に膨大な研究費を投じた開発競争が行われる中，日本人研究者も常にその存在感を示し続けて来た．しかしながら，全ての要請を満たす理想的なシンチレータは開発されておらず，最近でもPET装置などの医療画像装置や，非破壊検査装置，高エネルギー物理分野など様々な応用分野における小型化・高精度化のため，密度・応答速度・発光量などの点でこれまで以上の性能を持つシンチレータの開発に対して精力的な挑戦がなされている．

本報では，我々の新規シンチレータ結晶の開発などを例にして，発光中心の選択，発光波長に即した受光器の選択，シンチレータのアレイ化，アセンブリおよび2次元マップの撮像までを含め，放射線検出器として結実させるために辿る道程に関して報告する．

1. シンチレータ開発における発光中心の選択と母結晶の設計

1.1 シンチレータ

シンチレータの役割は$10^{5\text{-}6}$ eVのエネルギーを持つ単独の放射線を数eVのエネルギーを持つ複数の光子に変換することであり，放射線をシンチレータに当てると，この光子のエネルギーに対応した波長の光が得られることとなる．

1895年のレントゲンによるX線の発見により，人類は

[1] 東北大学 多元物質科学研究所　〒980-8577 宮城県仙台市青葉区片平 2-1-1
[2] 東北大学 未来科学技術共同研究センター（NICHe）　〒980-8579 宮城県仙台市青葉区荒巻字青葉 6-6-10
[3] 東京大学大学院工学系研究科　〒113-8656 東京都文京区本郷 7-3-1

放射線や放射性物質の存在を認識した．レントゲンは，放電管に数千ボルトの電圧をかけて陰極線の実験を行っていた際，偶然に放電管を厚い紙で覆っているにもかかわらず近くにおいてあった蛍光物質が発光している現象を発見し，放電管から目に見えないが物質に対する透過力をもった何かが発していると結論づけ，これをX線と名付けたとされる．この蛍光物質＝シンチレータであるので，シンチレータはそのシンチレーション現象により，人類に放射線および放射性物質の存在を教えてくれた物質とも言える．

1.2 発光中心の選択

シンチレータに求められる重要なパラメータとして，発光量，密度，蛍光寿命，エネルギー分解能等があるが，例えば，陽電子断層撮影（PET）においては，放射線（PETの場合はガンマ線）の数え落としを減らし，患者の絶対被曝量を低減させたいといったことから，近年のシンチレータ特性への要求として，特に“高速応答”がある．そのためには，シンチレータの蛍光寿命が短くなる必要があるが，同じ発光中心を用いる場合，蛍光寿命を短くすればするほど発光波長は短波長化する[11]．

$$\Gamma=\frac{1}{\tau}\propto\frac{n}{\lambda_{em}^{3}}\left(\frac{n+2}{3}\right)^{2}\sum_{f}|<f|\mu|i>|^{2} \quad \cdots(1)$$

ここで，Γは遷移確率，τは蛍光寿命，nは屈折率，λemは発光波長，fは終状態，iは始状態，μは双極子演算子である．

シンチレータに用いられる発光は，A．添加物のないワイドバンドギャップ材料におけるIntrinsic（self-activated）な発光と，B．添加物を用いたワイドバンドギャップ材料におけるExtrinsic（activated）な発光，とAとBの混合型のような位置づけに当たるC．直接遷移型のワイドバンドギャップ半導体のエキシトン発光とに大別される．

Aの Intrinsic（self-activated）な発光は，添加物のないワイドバンドギャップ材料のホスト自体からの発光であり，PbWO4，CaWO4，CdWO4などの“Self-trapped exciton発光”（STE発光）と，BaF_2の短寿命成分に代表される“Core-Valence発光”（CVL）とが挙げられる．BaF_2は蛍光寿命の短い成分としてSTE発光も有することが知られている．

Bの添加物を用いたワイドバンドギャップ材料におけるExtrinsic（activated）な発光は，更に5つに分類される．①代表格はCe: LSO，Ce: GSOなど，最先端のPET用シンチレータで用いられている“3価の希土類イオンの5d-4f遷移に伴う発光”である．これはパリティ許容遷移で，且つ，スピン許容遷移であるため，発光量が多く，蛍光寿命が短いという，応用面からとても好ましい特徴を有する．②Eu^{2+}を賦活剤として用いるシンチレータは“2価の希土類イオンの5d-4f遷移に伴う発光”に分類される．この発光はパリティ許容遷移だが，スピン禁制遷移であるため，Ce系に比して蛍光寿命はやや長めである．③Tl^{+}やPb^{2+}，Bi^{3+}などを賦活剤として用いるシンチレータは”6s 6p-6s^{2}遷移に伴う発光”に分類される．この発光はパリティ許容遷移，スピン禁制遷移だが，スピン軌道相互作用で補償されるため，蛍光寿命は①よりは長いものの，②よりも短い．④パリティ許容遷移で，且つ，スピン許容遷移の発光として，”電荷移動状態からの遷移に伴う発光”も挙げられる．近年，Ybの電荷移動状態からの遷移に伴う発光が話題となった．⑤蛍光体として用いられているTb^{3+}やEu^{3+}，Pr^{3+}などのシンチレータは“3価の希土類イオンの4f-4f遷移に伴う発光”に分類される．これはパリティ禁制遷移で，且つ，スピン禁制遷移であるため，蛍光寿命は長寿命である．

Cの直接遷移型のワイドバンドギャップ半導体のエキシトン発光は以下の3つに分類される．①無添加のZnOやPbI_2などで観察される“ワニエ励起子による発光”，②Ga: ZnO，In: ZnOなど，添加物を介して再結合が行われる”添加したイオンを介した電子と正孔の再結合に伴う発光”，③量子効果が顕著になるサイズのナノ結晶からのエキシトン発光．

従来，シンチレータは放射線の侵入長を考えた時，ある程度以上の大きさが期待されるため，量子効果が顕著になるような小さなサイズの物質を対象とした研究はあまり盛んではなかったが，最近のナノ領域への集中的な研究費の投入により，近年は③の研究に関する報告も大幅に増加している．

1.3 母結晶の設計と探索

母結晶は発光中心が入りやすいものを選ぶことが原則となる．ガンマ線やX線用であれば，有効原子番号の高いものが格子を構成する元素であるのが好ましい．一方，中性子用であれば，^{6}Li，^{10}Bといった中性子に対する散乱断面積の大きな元素で格子を構成するのが望ましい．なお，母結晶は発光波長において透明であることは必須である．

探索に我々が用いる方法論は以下の流れとなる．

①まずは情報収集と設計

(a) 母結晶候補となる酸化物・フッ化物のリストアップを行なう．

(b) 上記リスト中の物質が含まれる相図をデータベース（Phase Equilibria Diagrams（CD-ROM): The American Ceramic Society）から検索し，化合物候補を絞りこむ．

(c) 物性が有望な材料で，融点が高過ぎる，もしくは調和溶融組成から少しずれているものなど，融液成長が難しいものに関しては，Bond-Valence-Sumなどからの推測に基づき，同種異種原子価置換を試み，溶融組成，融点の調整を行なう．

②μ-PD法による単結晶試作

(a) 推論により候補とした母結晶組成において比較的早めの速度での結晶成長を試み，その際の必要な熱量

の変動から最適組成を検討する．変動が大きい場合は調和溶融組成からずれていると判断し，粉末X線回折法を用いた分析や走査型電子顕微鏡（SEM）の反跳電子像（BEI）の観察と合わせて最適組成を決定する．

(b) 同種の結晶を種結晶とするのが好ましいが，入手困難な場合は結晶構造が近く，構成元素も近い結晶を種結晶とする．不可能な場合はIr, Pt, W等を種結晶として，まずは結晶を作製し，そこから種結晶を切り出す．

(c) 種結晶は優先成長方位，熱膨張係数などを考慮し，方位を選定する．

(d) 結晶化率100％になるまで作製し，添加物の偏析等をチェックする．

(e) 特性評価用に，添加物の比率を変えた試料を準備する．

③光学特性の評価

光学評価は，試験片を寸法，2 × 2 × 10 mmの板状に加工・光学研磨し，まずは透過率測定を行う．次に，Photoluminescenceによる発光波長，蛍光寿命の測定を行う．シンチレータ用結晶の場合は更にX線励起のRadioluminescence発光波長の測定を行い，γ線励起のRadioluminescenceによる発光量特定，蛍光寿命の測定を行う．

②，③は常にフィードバックを掛け合いながら，迅速スクリーニングを執り進める．

1.4 Pr系新規シンチレータ材料の探索例

Pr^{3+}は，許容遷移である$4f^15d^1$-$4f^2$遷移と，禁制遷移であるf-f遷移とを持ち，ホストによっては数十nsと短い蛍光寿命を持つ5d-4f遷移による発光を示す．通常，Prはそのf-f遷移が良く知られており，蛍光寿命の長い発光成分が蛍光体などに用いられているが，最新の研究では，中程度に強い結晶場（Pr^{3+}の5d準位の一番低いエネルギーレベルが$^1S0$のレベルよりも低いという条件を満たす結晶場）の中ではPr^{3+}の5d-4f遷移に基づく発光が観察されることが注目されている．これまでにYAG，LuAG，YAP，YSO，LSO等の酸化物12, 13）に加え，フッ化物においても，KY_3F_{10}(KYF)[14]においてPr^{3+}の5d-4f遷移による発光が得られることが確認されている（図1）．

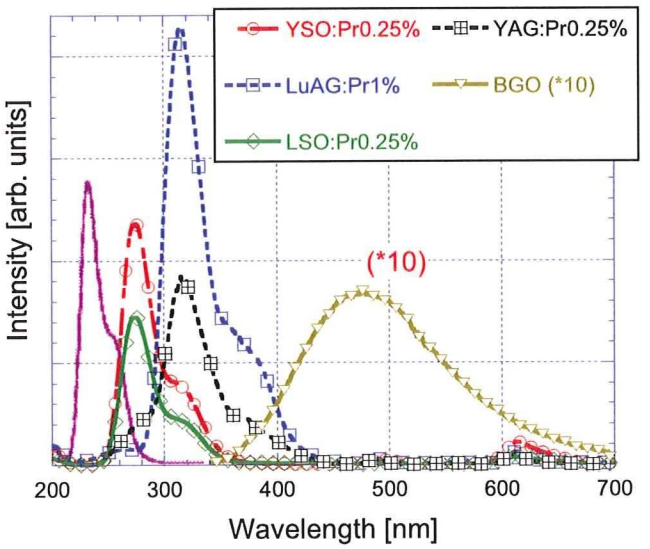

図1　YAG, LuAG, YAP, YSO, LSO, およびKYFホストにおけるPr^{3+}の5d-4f遷移によるX線励起発光スペクトル

特に我々の研究室にて開発されたPr: LuAG[15-16]の特性は優れており，発光量はBGOの数倍，蛍光寿命は約20 nsという短い値を示している．加えて，エネルギー分解能が他のPET用シンチレータに比して高いという特性を有している（表1）．

また，バルク単結晶成長も比較的容易であり，2インチ技術が確立している（図2）ので，共同研究企業である古河機械金属㈱において，有償でのサンプル出荷が開始されている．また，JST地域資源活用促進プログラムにて乳癌用PET（Positron Emission Mammography: PEM）の実機搭載プロジェクトやNEDO大学発事業創出実用化研究開発事業におけるMRI-PET用センサーに搭載されることとなった．

2. 受光素子の選択

これまで述べてきたように，シンチレータの役割は10^{5-6} eVのエネルギーを持つ単独の放射線を数eVのエネルギーを持つ複数の光子に変換することである．これらの

表1　PET用シンチレータの特性比較

	Pr: LuAG	Ce: GSO	Ce: LYSO	BGO
エネルギー分解能（%@662 keV）	4.60 %	8 %	8 %	10 %
蛍光寿命（ns）	20	40 ～ 60	40	300
発光量（ph/MeV）	18000	12500	33000	8000
密度（g/cm³）	6.7	6.7	7.4	7.13
発光波長（nm）	310	430	420	480

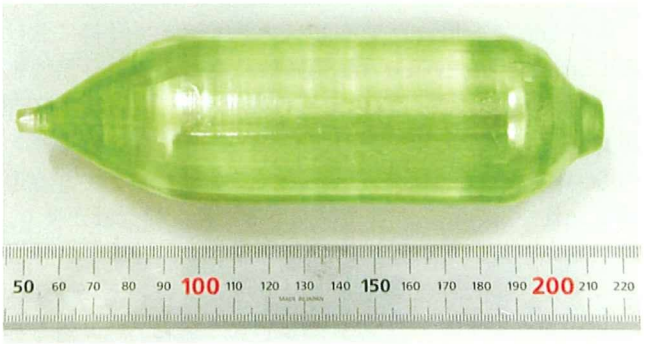

図2　Pr: LuAGの2インチ単結晶

光子は受光素子において光電効果によって電子に変換され，増幅過程を経た後に取り出され，電気信号として始めてPCなどで利用可能なデータとなる．充分な注意が払われないケースがしばしば見受けられるが，受光素子の感度は強い波長依存性を持つ．そのため実際の放射線検出器を開発する際には，シンチレータの発光波長に対して相性の良い受光素子を選択することが重要である．図3に，代表的な受光素子の量子効率を示す．分野によって量子効率の定義は異なるが，この場合の量子効率は，受光素子に入射した光子が電子に変換される割合であり，100 %に近ければ近いほど良い．

現在最も広く利用されている受光素子は光電子増倍管（PMT）である．PMTは20世紀初頭の開発以来，幾多の改良が重ねられ，非常に使いやすい受光素子となっている．典型的には，波長400 nm前後の青色光に対して20-30 %の量子効率（Quantum Efficiency: QE）を持ち，10^6倍と非常に高い増幅率を持つことが特徴である．

近未来の受光素子として開発が進められているものが，Si-APDと呼ばれる半導体素子である．図3に示すように，400-800 nmという広い範囲において，QE > 80 %と極めて高い値を示している．そのためエネルギー分解能重視の応用を考えた場合，Si-APDを用いるべきである．一世代前は，Si-PDが用いられていたが，これは高いQEの反面，内部増幅機構がなく，S/Nを高めることが出来なかった．この弱点を克服し，$10^{2\text{-}3}$倍の増幅率を持たせたものがSi-APDである．PMTと比較した場合，小型，軽量，省電力，磁場中動作可能など優れた面が多いが，増幅率が低いため利用するには放射線物理実験における高い技術力が必要となり，本邦では一部の研究者しか使いこなせない．我々は，Si-APDを二次元配列化し撮像能力を持たせ，我々の開発したPr: LuAGと組み合わせることで，次世代PET-MRIを実現すべく研究を行っている．Si-APDの次世代器としては，ガイガーモードAPDがあり，これも10^6倍と高い増幅率を示す．しかしながら，入力エネルギーと出力波高値の線形成が保たれていないため，今後の開発に期待する部分が大きい．我々の研究室においても基礎実験は行っているが，上記の線形性に加え，温度・高電圧に対する強い依存性を如何に補償するかも今後の課題であろう．同様に，半導体素子としてはGaN系，SiC系，ダイヤモンド系などの受光素子も考えられるが，未だ微弱光測定における実用レベルには至っていない．また，シンチレータに求められる重要なパラメータとして，挙げた発光量，密度，蛍光寿命，エネルギー分解能等があるが，その優先順位は受光器によって異なる．従来の位置敏感型光電子増倍管（PS-PMT）を用いる場合，電荷重心演算により位置特定を行うため，発光量が最重要特性とされる．そのため，PS-PMTを受光器とした場合，シンチレータは発光量に優れるCe: LYSOが有利である．一方，APDとの組合せの際は，シンチレータと検出器が1対1の対応となるので，発光量はある程度以上確保されていれば良く，エネルギー分解能が高いことが要求される．Pr: LuAGはエネルギー分解能が4.6 %と高く，APDを受光器として用いる場合は，LYSOに比しても有利である．

PMT登場以前に，放射線を検出していた素子はガス検出器であった．電離エネルギーが数eV程度のガスを充満させ，放射線が突き抜ける際の電離を利用して，高電場を印加することで$10^{3\text{-}4}$程度まで増幅した後に信号を検出する形式である．PMT登場後は，PMT＋シンチレータに比べ著しく検出効率が低いため，あまり利用されなくなっていたが，近年，これとシンチレータを組み合わせる基礎実験が行われている．受光素子として用いた場合，一般的には波長100-200 nm（VUV）に感度を持つ（図3中TEA, TMAE）．比例計数管など過去のガス検出器は応答速度が遅い（数マイクロ秒）などの問題があったが，最近では均一に高電場を印加できるように改良が加えられ，その問題

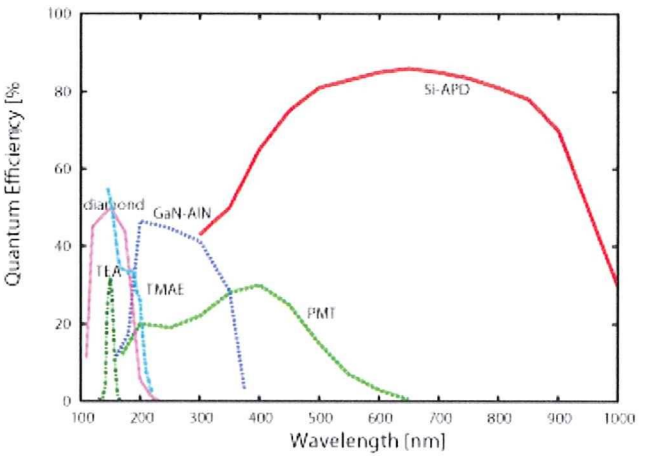

図3　代表的な受光素子の量子効率

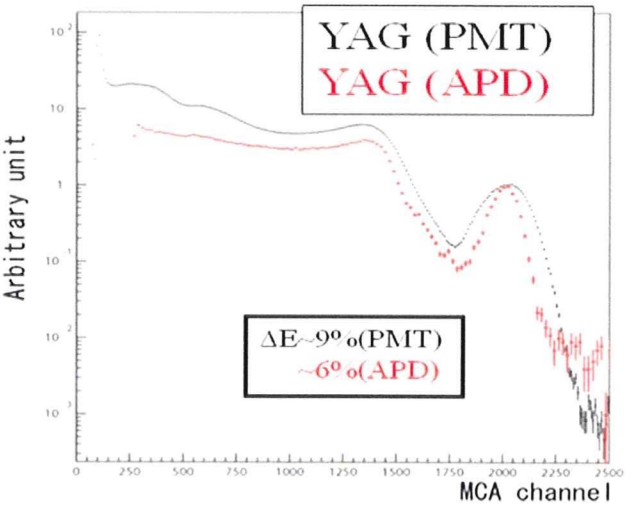

図4　Ce: YAG（発光波長520 nm）のAPD, PMTによる読み出し

も克服されつつある．そのため仮にVUVで発光するシンチレータが発見された場合，極めて安価・大面積の放射線検出器を構成できる可能性がある．

以上述べてきたように，シンチレータに最適な受光素子を選択することは重要である．図4はその一例であり，^{137}Csを照射した際のガンマ線スペクトルである．シンチレータはCe: YAG（発光波長は520 nm）であり，当然APDが最も適した受光素子である．図から明らかなように，APD読み出しの方が著しく（1.5倍）エネルギー分解能（FWHM）が良い．即ち，もしも不適合な受光素子を選択した場合，シンチレータの持つ潜在能力が全く発揮されず，折角開発した材料も世に埋もれてしまう危険性があることを示している．材料開発研究に従事する研究者は注意すべきである．

3. シンチレータのアレイ化，アセンブリおよび2次元マップの撮像

「材料は使われて初めて“材料”と呼ばれる」と考えると，開発したシンチレータはアレイ化し，受光素子とアセンブリして二次元の放射線イメージを取得し，ガンマカメラとして動作するところまで辿り着きたい．1.4 Pr系新規シンチレータ材料の探索例に示す通り，我々は，Pr: LuAGでこれを具現化する機会を得た．しかしながら，道のりは平たんではなく，まず，反射材の選択から考え直す必要性に直面した．

3.1 反射材の選択とアレイ化

一般的に反射材としては，テフロンやESRフィルムが用いられている．ここで，Pr: LuAGはこれまで用いられてきた多くのシンチレータが可視光発光（400-500 nm）するのに対し，紫外発光（310-370 nm）することが特徴である．この場合，従来用いられてきた誘電体多層膜反射材は紫外線を吸収してしまうため，最適な反射材の選択が必要となる．

Pr: LuAGの特性を最大限に引き出すためにも，反射材の開発が必須となり，我々は色々な候補の中から硫酸バリウムを反射材として用いることで，従来の反射材実装時に比べ，最終的な取り出し発光量の40 %向上を達成した．当該アレイ化実装技術は従来の手法に比べて非常に簡便かつ高精度であり，今後量産化を行う上で欠かせない基盤技術となった．Pr: LuAGのアレイを図5に示す．

3.2 アセンブリおよび2次元マップの撮像

Pr: LuAGアレイと位置敏感型光電子増倍管（PSPMT）をアセンブルし，二次元の放射線イメージを取得し，その解像度評価を行った．実験室レベルにおいては，PSPMT-H8500（浜松ホトニクス社製）との組み合わせにおいてFWHMで約1 mmの解像度が得られており，これは市販されているPET装置の5-10倍の解像度に達している．

図6に取得した放射線二次元イメージを示す．本研究は，大学側の研究者はシンチレータ材料の発見，反射材の発見，二次元イメージの定量評価などの基礎的研究において貢献し，古河機械金属株式会社はその量産化手法の開発に注力するという理想的な形での産学連携が行われたことにより，材料の開発からわずか3年程度で，実機搭載プロジェクトがスタートし，アセンブリ技術や二次元撮像の成功まで達成した．

PEM装置は，東北大学サイクロトロンRIセンター，東北大学病院，仙台画像検診クリニック，神戸高専らの協力のもと順調に開発が進行しており，2008年夏にプロトタイプの完成が予定されている．

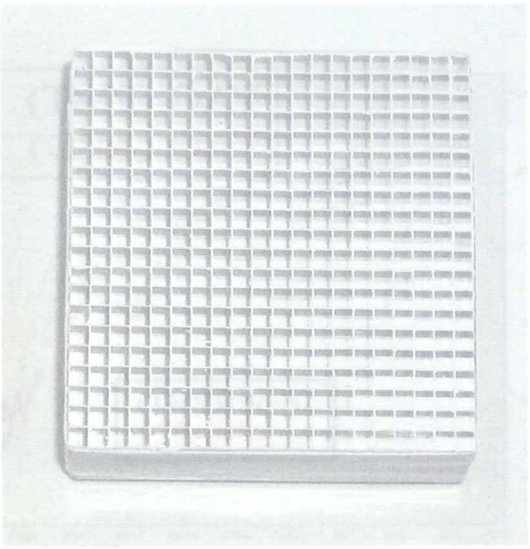

図5 Pr: LuAGで作製した20 × 20 pixelブロックアレイ（1 pixelのサイズは2 × 2 mm）

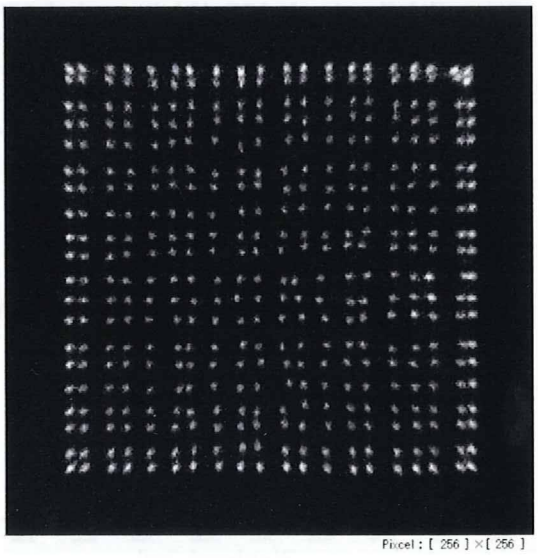

図6 Pr: LuAGアレイとPSPMTをアセンブルして取得した二次元の放射線イメージ

4. まとめと今後の展望

現行の全身PETではX線CTの形態情報とPETの機能情報を組合せたPET-CTが主流である．これはPETは機能情報（がんの代謝活動の把握等）の取得に優れるものの，解像度（汎用機で5 mm程度）が悪く形態情報が不十分である一方，X線CTは機能情報は得られないものの，解像度は500 μm以下と高解像度であるためであり，最先端の医療画像装置では，PET像とCT像を組合せた画像が用いられている．しかしながら，最近，X線CTはPETに比して10倍程度の大きな放射線被曝量が問題視されて来た．そのため，形態情報を得る手段として，X線CTの代わりに解像度が数十 μm程度かつ 血流などの動態観察も可能であるMRIが注目され，MRIとPETの組合せによるMRI-PETの実用化の要請が高まっている．この次世代のPET装置であるMRI-PET用を考えた場合，受光素子としては磁場不感であるAPDが必須となる．（PMTではシグナル増幅過程で電子が長距離進むため，MRIの磁場の影響を受けて像が歪んでしまう．）

ただし，Si-APDを用いたPETを具現化する際の問題点は幾つかある．大別すると以下の二つであろう．一つ目は取り扱うのにPMTの場合と比べ格段に高い技術力が要求され，世界の大半の研究者にとって参入するには敷居が高いことである．二つ目は，多素子型のSi-APDは未だ開発されておらず，撮像検出器の開発には，これを開発せねばならないことである．この技術的に大きな難問に対し，我々は多素子型SI-APDを用いたPr: LuAGガンマカメラの開発という，正に真っ向から挑む研究を企画している．幸いにもNEDO大学発事業創出実用化研究開発事業「MRI-PET用Pr: LuAG + APDアレー放射線検出器システムの開発」が開始されるに至った．東大，東工大，放医研，仙台画像検診クリニックと共に3年以内の実用化を目指す研究として，2008年4月よりスタートした．Pr：LuAGシンチレータを用いたアレイ化技術が確立しており，Si-APDアレイとのアセンブリ試験中である．加えて，Pr：LuAGおよびSi-APDの性能に特化した独自のASIC開発も行っており，アセンブリ試験後には実際に磁場中での放射線応答測定も予定している．

謝辞

JST地域資源活用促進プログラム，NEDO大学発事業創出実用化研究開発事業のメンバーの多大なご協力を感謝申し上げます．特にプロジェクト企画初期段階からの主要共同研究者である薄善行氏，鎌田圭氏に感謝申し上げます．また，シンチレータの発光メカニズム等を議論するにあたり多大な支援を頂いたチェコ科学アカデミーM. Nikl氏，デルフト工科大学のP. Dorenbos氏に謝意を表します．

参 考 文 献

1) R. Hofstadter: Phys. Rev. **74** (1948) 100
2) R. Hofstadter: Nucleonics **6** (**5**) (1950) 70
3) J.B. Czirr, E. Catalano, Nucl. Instr. & Meth. **A143** (1977) 487
4) E. Sakai: IEEE Trans. Nucl. Sci. **NS-34** (**1**) (1987) 418
5) W.W. Moses, S.E. Derenzo, Nucl. Instr. & Meth. **A299** (1990) 51
6) V.G. Baryshevski et al., Nucl. Instr. & Meth. **A322**, (1992) 231
7) M. Kobayashi, M. Ishii, Y. Usuki, H. Yahagi, Nucl. Instr. & Meth. **A333** (1993) 429
8) K. Takagi, T. Fukazawa: Appl. Phys. Lett. **42** (**1**) (1983) 43
9) C.L. Melcher, U.S. Patent No. 4,958,080, 1990
10) C.L. Melcher, J.S. Schweitzer: Nucl. Instr. & Meth. **A314** (1992) 212
11) Dorenbos: Nucl. Instr. Methods Phys. Res. **A486** (2002) 208
12) A. Yoshikawa, M. Nikl, G. Boulon and T. Fukuda: Opt. Mat. **30** (2007) 6
13) M. Nikl, A. Yoshikawa, A. Vedda and T. Fukuda: J. Cryst. Growth **292** (2006) 416
14) A. Yoshikawa, K. Kamada, M. Nikl, K. Aoki, H. Sato, J. Pejchal and T. Fukuda: J. Cryst. Growth **285** (2005) 445
15) M. Nikl, H. Ogino, A. Krasnikov, A. Beitlerova, A. Yoshikawa and T. Fukuda： Phys. Status Solidi **A202** (2005) R4
16) H. Ogino, A. Yoshikawa, M. Nikl, A. Krasnikov, K. Kamada, and T. Fukuda： J. Cryst. Growth **287** (2006) 335

(2008年6月26日受理)

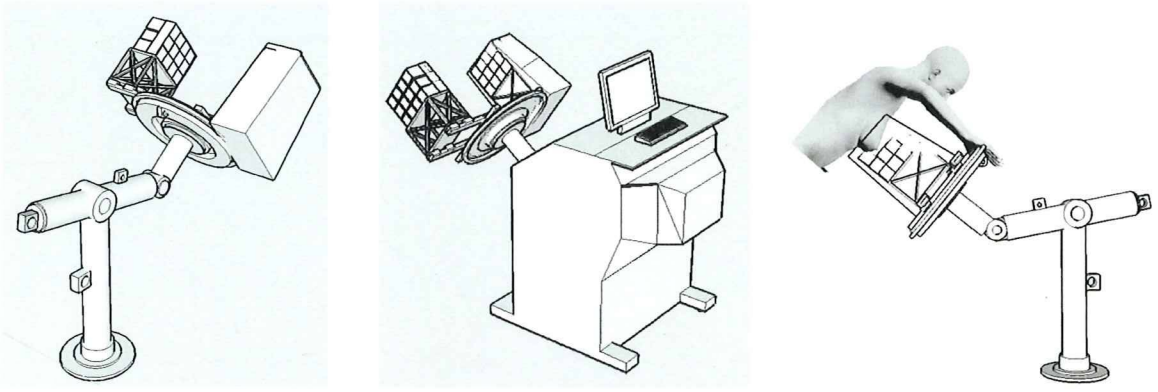

図7 PEM装置の外観

Review Article

Development of Novel Scintillator Crystals and Embodiment as Radiation Detector; from Selection of Luminescent Mechanism, Suitable Photo-detector, Making Scintillator Array, Assembly to 2 Dimensional Imaging.

Akira Yoshikawa[1,2], Takayuki Yanagida[1], Yuui Yokota[1], Hiraku Ogino[3]

On the study to develop novel scintillator crystal, they focus mainly on selection of emission center and host lattice. However, for the practical use as radiation detector or medical imaging system, arraying and assembling technology is required. Only after those processes, the two dimensional imaging is obtained. In this report, we report on the design rule of novel scintillator crystal as well as the way toward the two dimensional imaging.

[1] Institute of Multidisciplinary Research for Advanced Materials (IMRAM), Tohoku University 2-1-1 Katahira, Aoba-ku, Sendai, Miyagi 980-8577 JAPAN

[2] New Industry Creation Hatchery Center (NICHe), Tohoku University 6-6-10 Aoba, Aramaki, Aoba-ku, Sendai, Miyagi 980-8579, JAPAN

[3] School of Engineering, The University of Tokyo 7-3-1 Hongo, Bunkyo-ku, Tokyo, 113-8656, JAPAN

Measurement of Light Yield of Ce^{3+} Perturbed Emission of CaF_2 Scintillator coupled with Avalanche Photodiode

Takayuki Yanagida, Kyoung Jin Kim, Kei, Kamada, Kenji Aoki,
Noriaki Kawaguchi, Kentaro Fukuda, M. Sato, and Akira Yoshikawa

Abstract–**The present work describes the first detailed gamma-ray responses of Ce^{3+} perturbed emission in CaF_2 host. Ce^{3+} 1%,, 3%, 5%, 10%, and 20% doped single crystalline CaF_2 scintillators were grown by μ-PD method. Their transmittance were measured by JASCO V550 spectrometer, and about 80% transparence was achieved. All the sample showed an emission peak around 330 nm, which was Ce^{3+} perturbed emission, when they were irradiated by 1GBq ^{137}Cs and read out by CCD. Absolute lihjt yield (ph/MeV) was measured by Si-APD (S8664-55, Hamamatsu), and the 3% sample showed the highest light yield around 900 ph/MeV with 2 μs shaping time. The decay time was measured by FLS900 (Edinburgh instrument), and about 40 ns decay was observed.**

I. Introduction

CaF_2, a fluorite is a famous emission material, and is utilized to many optical applications as a lens. In 1960's, it was reported that Ce^{3+} doped CaF_2 emitted scintillation light [1][2]. As Ce^{3+} ion resides at the Ca^{2+} site, there is a need for a charge compensation, which is accomplished by an interstitial F^- ion at the vacant cationic sites of the cubic CaF_2 lattice. Depending on the position of F^-, the Ce^{3+} centers with tetragonal C_{4v} (nn position of F^-) or trigonal C_{3v} (nnn position of F^-) symmetry are created [3]. The former center is dominating and its absorption bands are found at about 307 nm (4f-5d(e_g)) and 190-210 nm (4f-5d(t_{2g}), while its luminescence occurs in typical Ce^{3+} double peak spectrum at 318 nm and 339 nm with a decay time around 40 ns [4]. At that time, Ce^{3+} concentration in CaF_2 host is less than 1 %, and gamma-ray response was not evaluated.

In the present work, we develop Ce:CaF_2 scintillators with a different Ce^{3+} concentration of 1%, 3%, 5%, 10%, and 20%, by μ-pilling down (μ-PD) method, and evaluate absolute light yield when coupled with Si-avalanche photodiode (Si-APD) S8664-55 manufactured by Hamamatsu Photonics. Also, photoluminescence decay time is measured by FLS 900 (Edinburgh Instrument). Finally, a dependence of Ce^{3+} to those physical properties are summarized.

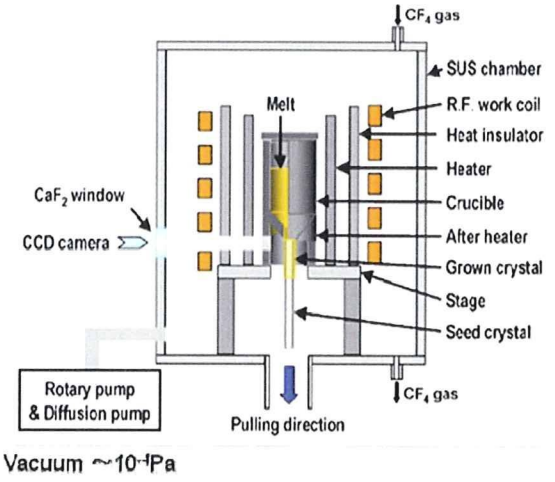

Fig. 1. A schematic drawing of μ-PD equipment.

II. Experiment

In this section, we briefly explain about experimental setups. They are widely separated to three parts, of which one is crystal growth part, optical measurement part, and gamma-ray responses part.

A. Crystal Growth

Single crystals of solid solution between CeF_3 and CaF_2 were grown by the micro-pulling-down (μ-PD) method. The description of this method can be found in [5, 6]. Starting materials were prepared from the stoichiometric mixture of 99.99% pure CeF_3 and CaF_2 powders produced by Stella Chemifa Corporation. They were thoroughly mixed and put into a graphite crucible. The chamber was evacuated up to 10^{-4} Torr. Then, the crucible was heated up to 600 °C and kept for about 1 hour at this temperature in order to remove oxygen traces caused by moisture of raw materials and adsorbents on the chamber surface. During this baking procedure, the

Manuscript received November 4, 2008. This work was supported in part by the Hatano foundation in IMRAM, Tohoku University, and The Murata Science foundation. .

T. Yanagida, K. J. Kim, M. Sato, and A. Yoshikawa are with the IMRAM, Tohoku University, Sendai, Japan (telephone: +81-22-217-5167, e-mail: t_yanagi @tagen.tohoku.ac.jp).

K. Kamada is with Furukawa Co. Ltd., Tsukuba, Japan (telephone: +81-22-217-5167, e-mail: k-kamada@furukawakk.co.jp)

N. Kawaguchi and K. Fukuda are with Sendai Research and Development Center of Tokuyama Co. Ltd., ICR-building, Minamiyoshinari, Aoba-ku, Sendai, Japan (telephone: +81-22-217-5167, e-mail: famicom @tagen.tohoku.ac.jp).

K. Aoki is with the Stella Chemifa Corporation, 1-41 Rinkai-cho, Izumiootsu, Osaka 595-0075, Japan.

chamber was further evacuated down to 10^{-5} Torr. After the baking, the recipient was filled with high purity Ar gas (99.999%) and CF_4 gas (99.999%) until ambient pressure. The crucible was heated up to about 1400 °C above the melting temperature of CaF_2. CaF_2 single crystal grown by Cz method was used for the seed. The growth rate was 0.02-0.5 mm/min. By this processes, Ce 1%, 3%, 5%, 10%, and 20% doped crystals were prepared. Figure 1 exemplifies a set up of μ-PD equipment.

B. OpticalMeasurement

A transmittance was measured by JASCO V550 spectrometer between 200 and 650 nm ranges. A wavelength resolution was set to be 1 nm. Then, emission wavelength was measured by PMA-12 CCD camera, made by Hamamatsu. The excitation source was 1 GBq ^{137}Cs gamma-ray source, which can excited the host material of scintillators. Generally, a luminescence spectrum are obtained by UV excitation which can only excited emission centers, but in actual experiments, excitation is done by radiation sources. Thus, the present experiment provides a very similar situation to the scintillaion processes. Additionally, in some literature (e.g., [7]), the result that emission wavelength shows a little difference according to excitation sources (UV, X-ray, gamma-ray, charged particles, and so on) was reported.

C. Scintillation Property Measurements

First, we evaluated the absolute light yield by a coupling with Si-APD (S8664-55, Hamamatsu). Scintillators are optically coupled with APD by optical grease (OKEN 6262A). The sample was wrapped by Teflon tape. The APD has a 5 mm × 5 mm light sensitive window, and ~ 40% quantum efficiency around 300 nm, which is an emission peak of Ce:CaF_2. Light yields were evaluated by ^{137}Cs 662 keV photo-peak, compared with a direct irradiation to Si from ^{55}Fe 5.9 keV X-ray, which generates 1640 electron-hole pairs. After a correction of quantum efficiency at the emission wavelength, we can obtain an absolute light yield. The experimental temperature was controlled at +20 ± 0.5 °C.

Then, a photoluminescence decay measured by FLS900 (Edinburgh Instrument) was investigated. Because of a tiny size, and low stopping power of our products, it is difficult to measure their decay time by gamma-ray irradiation. By this reason, we evaluated decay time by photoluminescence. Generally, photoluminescence results are little bit difference with gamma-ray excited decay times, but for decay time, they agree within few nano seconds, which will be due to a energy migration time from host to emission centers.

III. Experimental Results

A. Crystal

The as grown crystals were transparent, 2.0 mm in diameter and around few cm length. Neither visible inclusions nor cracks were observed. Crystals were cut along the growth axis and polished with 0.3μm diamond paste. Obtained plate with the dimension of 2.0ϕ ×3.0 mm^3 is used for the optical and gamma-ray experiments. Figure 2 exemplifies the Ce 5% doped sample.

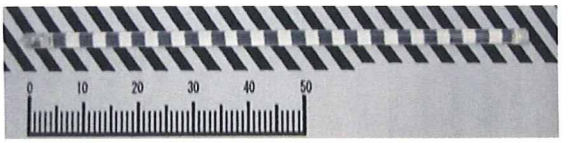

Fig. 2. Ce^{3+} doped CaF_2 scintillator grown by μ-PD method.

B. Optical Properties

By using JASCO V550, transmittance between 200 and 650 nm of these sample pieces were obtained, as shown in figure 3. They all showed a similar result, where 70-80% transparency was observed in the wavelength longer than 320 nm. Only the 1% sample showed few % transparency around 280 nm, which will be attributed to a smallness of an amount of absorption ions. The accuracy of the transmittance was few % in this equipment.

Then, gamma-ray excited emission spectra were studied, as shown in figure 4. The emission peaked around 330 nm and broadened from 290 nm to 400 nm. The exposure was set to be 30 s for each measurement. From these measurements, it was revealed that the shorter wavelength emission was self-absorbed by the scintillator itself. In the same experimental procedures, the 20% doped sample showed the strongest emission intensity.

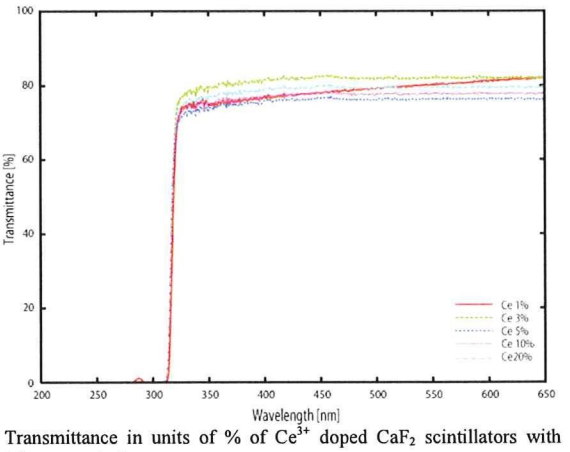

Fig. 3. Transmittance in units of % of Ce^{3+} doped CaF_2 scintillators with different Ce concentrations.

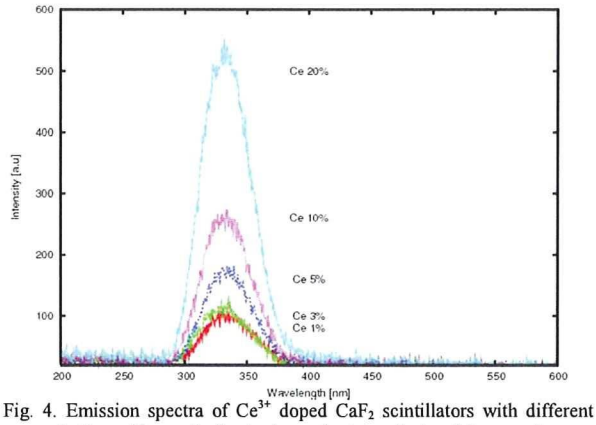

Fig. 4. Emission spectra of Ce^{3+} doped CaF_2 scintillators with different Ce concentrations. The vertical axis shows the intensity in arbitrary units.

C. *Scintillation Properties*

By using APD S8664-55, we measured gamma-ray spectra. Figure 5 exemplifies the 5% doped sample irradiated by ^{137}Cs, where 662 keV photoabsorption peak and the Compton edge were clearly detected. The continuous component shown in the figure is attributed to the Si direct detection of radiation, which is sometimes observed in such measurement when the scintilaltor has a small dimension or low stopping power. This specific APD has a depletion layer of about 10 μm thickness, and it can detect low energy (10-20 keV) X-rays.

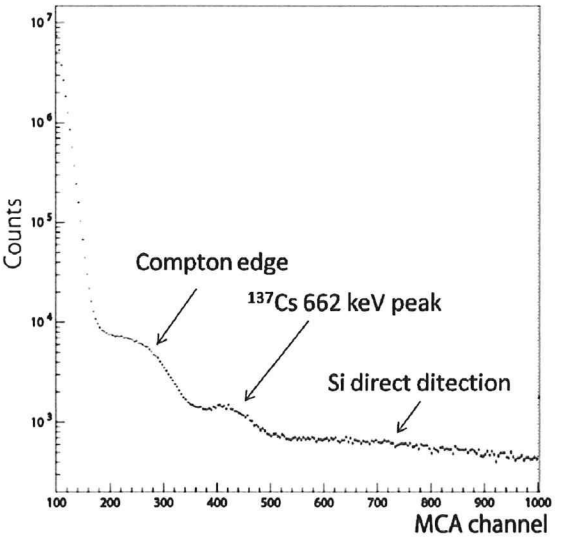

Fig. 5. Gamma-ray spectrum of 5% doped sample when ^{137}Cs is irradiated.

We fitted the photoabsorption peak by a single component Gaussian function, and determined the peak channel. By compared with the peak channel with the 5.9 keV peak from ^{55}Fe source, which can create about 1640 electron-hole pairs, we can calcurate the electron-hole pairs created by Ce:CaF_2 scintillation lights. After a correction by the quantum efficiency of the APD, which shows about 40% around 330 nm, we can obtain an absolute light yield of the scintillators.

Figure 6 shows the light yield plotted against the Ce concentration. The optimum Ce concentration is inferred to be 5 mol% for 2 mm thick Ce:CaF_2s.

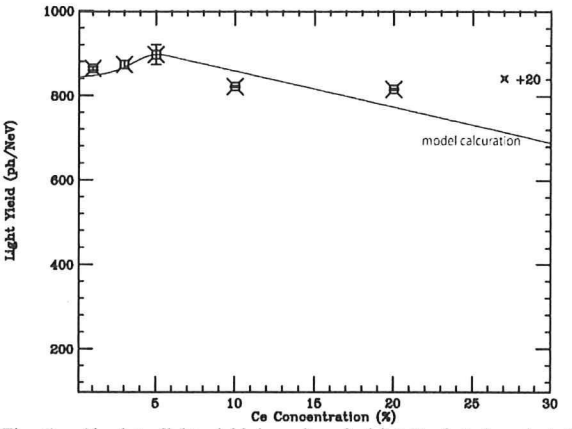

Fig. 6. Absolute light yield in units of ph/MeV plotted against the Ce concentration.

The photoluminescence decay was measured by FLS900. The excitation wavelength was set to be 290-310 nm, and the emission was 320-340 nm. Figure 7 shows an example of the decay curve of Ce 20% doped sample, where the dotted line represents the one component exponential fitting function, because generally the PL decay only shows the emission caused by one excitation pass.

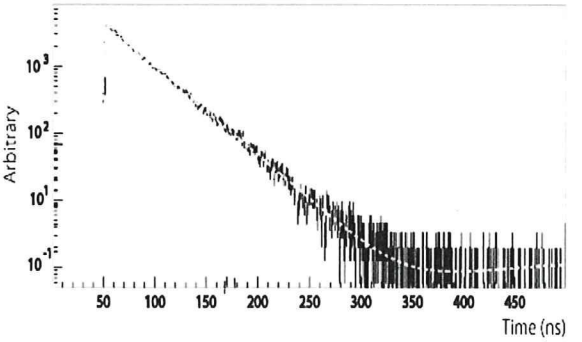

Fig. 7. Photoluminescence decay of Ce 20% doped one. .

In the same way, we obtained the scintillation decay properties of all the sample pieces. Figure 8 shows the relation between a decay time and the Ce concentration. As shown in this figure, more Ce concentration increases, the more decay component becomes faster. As the Ce concentration increases, the decay time will be faster up to few nsec, which is the decay time of CeF_3.

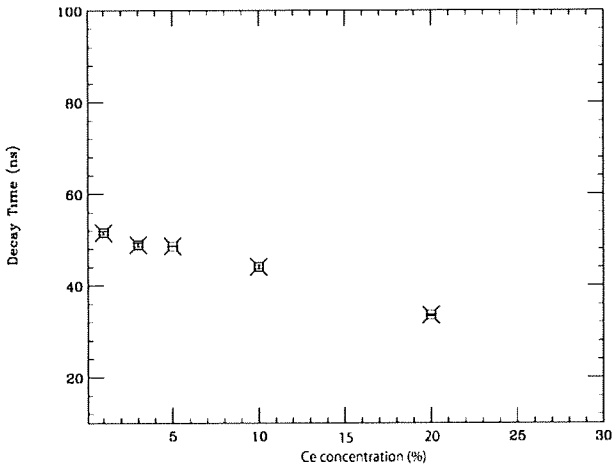

Fig. 8. Photoluminescence decay plotted against the Ce concentration.

IV. Conclusions

In the present work, Ce^{3+} perturbed emission in CaF_2 host was investigated. We successfully developed transparent Ce 1%, 3%, 5%, 10%, and 20% doped CaF_2 scintillators by μ-PD method. Generally, the perturbed emission shifts to the longer wavelength compared with the normal emission. In fluoride scintillator, Ce^{3+} emission generally happens at 280-290 nm (e.g., CeF_3 [8], Ce:$LiCaAlF_6$[9]). The present work shows the perturbed emission occurs around 330 nm, which is slightly longer than above values.

The absolute light yield of Ce:CaF_2 and the optimum Ce concentration when it is used as a scintillator, are first appeared. The optimum value turned out to be 5% and the absolute light yield is about 900 ph/MeV. The main component of the decay time was also measured and they were around 40 ns. Thus, Ce:CaF_2 will not be applied in the industrial purpose, because of its low light yield, and middle response speed as a scintillator. But this scintillator will be attractive in scientific purpose, including dark matter search [10].

Acknowledgment

This work was supported in part by the Murata Science foundation, and the Japan Securities Scholarship Foundation.

References

[1] M.J. Weber, R.W. Bierig: Phys. Rev. **134** (1964) A1492.
[2] J.M. Baker, E.R. Davies, J.P. Hurrel: Phys.Lett. **A 26** (1968) 352.
[3] W.J. Manthey, Phys.Rev. **B 8**, (1973) 4086..
[4] S.B. Mirov, A.Yu. Dergachev, W.A. Sibley, V.B. Sigachev, A.G. Papalashvili, T.T. Basiev, *Mat. Sci. Forum*,.
[5] A. Yoshikawa, T. Satonaga, K. Kamada, H. Sato, M. Nikl, N. Solovieva,T. Fukuda, J. Cryst. Growth, **270**, (2004) 427-432,.
[6] A. Yoshikawa, M. Nikl, G. Boulon, T. Fukuda, Opt. Mater. **30** (2007) 6-10.
[7] Joshua D. Kuntz, Jeffery J. Roberts, Meghan Hough, Nerine J. Cherepy, *Scripta Materialia*, Volume **57**, Issue **10**, (2007), 960-963
[8] P. Belli, R. Bernabei, R. Cerulli, C. J. Dai, F. A. Danevich, A. Incicchitti, V. V. Kobychev, O. A. Ponkratenko, D. Prosperi, V. I. Tretyak, Yu. G. Zdesenko, NIM-A, Volume **498**, Issues 1-3, (2003), Pages 352-361
[9] A. Yoshikawa, T. Yanagida, K. J. Kim, N. Kawaguchi, S. Ishizu, K. Fukuda, M. Nikl, M. Miyake, M. Baba, in the present conference N2-395.
[10] Yuki Shimizu, Makoto Minowa, Wataru Suganuma and Yoshizumi Inoue, Physics Letters **B 633** (2006) 195-200

Ce^{3+}およびPr^{3+}添加 $YLiF_4$、$BaLiF_3$、$LiCaAlF_6$ 結晶の放射線励起時における発光特性評価

柳田健之[A]、河口範明[A,B]、横田有為[B]、石津澄人[B]、福田健太郎[A,B]、藤本裕[A]、阿部直人[A]、吉川彰[A]

東北大学多元物質科学研究所[A]

トクヤマ研究開発部門仙台開発センター[B]

Luminescence properties of Ce^{3+} and Pr^{3+} doped $YLiF_4$, $BaLiF_3$, and $LiCaAlF_6$ crystals

T. Yanagida[A], N. Kiawaguchi[A,B], Y. Yokota[B], S. Ishizu[B], K. Fukuda[B], Y. Fujimoto[A], N. Abe[A] and A. Yoshikawa[A]

IMRAM, Tohoku University[A]

Research Lab.(Sendai), Research & Development Div., Tokuyama., Co. Ltd.[B]

We have investigated the radio-luminescence (RL) properties of Ce^{3+} and Pr^{3+} doped fluoride crystals, including $YLiF_4$ (YLF), $BaLiF_3$ (BLF), and $LiCaAlF_6$ (LiCAF). These crystals were grown by micro-pulling down method in diameter of 2 mmϕ and ~10 cm length for the radiation measurement applications. The dopant concentration of them was set to be 0.5mol% to the cation. After the growing process, they were cut and polished to have physical dimension of 1 ×2×7 mm^3. They all showed 80% transparency in near UV and visible wavelength. In order to study the luminescence property when radiation is irradiated, 1 GBq ^{137}Cs 662 keV gamma-ray was irradiated to them. As a result, Ce:YLF, Ce:BLF, and Ce:LiCAF showed a luminescence due to Ce^{3+} 5d-4f ($F_{7/2}$, $F_{5/2}$) transition around 300 nm. On the other hand, Pr^{3+} doped samples showed an intense line around 260 nm due to 5d-4f transition, and a lot of line between 400 and 600 nm due to 4f-4f transition.

1. はじめに

シンチレータ結晶は核医学(PET、X線CT)、資源探査、空港の手荷物検査機などのセキュリティ分野、原子力発電所におけるモニタ、宇宙・素粒子といった基礎物理など、広汎な分野で利用されている放射線検出器のメインデバイスである。シンチレータは一般に放射線を光電吸収などにより電子に変換するホスト物質と、その電子のエネルギーを発光に変換する発光中心元素から成る。近年では発光中心としてCe^{3+}、Pr^{3+}などの5d-4f遷移を用いるシンチレータが主流であり、特に酸化物ホストに関して幅広く研究が行われている。

これに対し、我々は次世代シンチレータデバイスとして、フッ化物単結晶の開発に着手している。フッ化物材料の利点としては、真空紫外から可視域にかける広い透明帯